CERFACS UNIVERSITÉ DE NANTES université angers

Shock capturing techniques for the Spectral Difference method

Author : Wioletta Stachura

Supervisors : G. Puigt, J.-F. Boussuge
University Supervisor : A. Crestetto

Ref.: WN-CFD-16-207
September 12, 2016

Centre Européen de Recherche et de Formation Avancée en Calcul Scientifique
42 avenue Coriolis – 31057 Toulouse Cedex 1 – France
Tél : +33 5 61 19 31 31 – Fax : +33 5 61 19 30 00
http://www.cerfacs.fr – e-mail: secretar@cerfacs.fr

Contents

Chapter 1

Introduction

This report describes the whole work done during the internship at CERFACS in the CFD team. At the beginning, the research center and the CFD team are presented. Then, the description of a field of interest for CFD called LES is introduced. Finally, the general principle of high-order spectral methods is recalled and the aim of the training period is given.

1.1 CERFACS

CERFACS (Centre Européen de Recherche et de Formation avancée en Calcul Scientifique) is a research organization that aims to develop advanced methods for the numerical simulation and the algorithmic solution of large scientific and technological problems of interest for research as well as industry, and that requires access to most powerful computers presently available. This research center is governed by a Conseil de Gérance with representatives from its associates, and benefits from the recommendations of its Scientific Council. CERFACS is strongly interacting with its seven shareholders:

- CNES, the French Space Agency,
- AIRBUS Group France, European Aeronautic and Defence Space Company,
- EDF, Electricité de France,
- Météo France, the French meteorological service,
- ONERA, the French Aerospace Lab,
- SAFRAN, an international high-technology group,
- TOTAL, a multinational energy company.

More than 150 people work at CERFACS, coming from ten different countries and who belong to five teams:

- Aviation and environment,
- Climate modeling and Global change (GLOBC),
- Computation Fluid Dynamics (CFD),
- Computer Support Group (CSG),
- Parallel Algorithms.

1.2 CFD team

The CFD team is composed of three main groups of work: combustion, turbo machinery and applied aerodynamics. It is the biggest team at CERFACS and represents approximately half of the research center in human resources. The aim of the CFD team is to solve the largest CFD problems by use of solvers with High Performance Computing (HPC) capability.

1.3 Large eddy simulation

The idea of Large Eddy Simulation (LES) is to compute the largest turbulent scales and to model the smallest ones. However, this technique demands highly accurate, low dissipation and low dispersion numerical methods to solve real-world problems. There are two possibilities which guarantee these three properties. The first approach consists in considering a lot of degrees of freedom (DoF) and a low-order approach. The number of DoF must be high in order to keep information over long distance, with both limited dissipation and dispersion. At CERFACS, it is preferred to take less DoF and to introduce a high-order technique, because for the same number of degrees of freedom, high-order methods give a less dissipative solution than their low-order counterparts. Although advanced schemes work well for LES, another family of techniques (high-order spectral methods), which are suitable for HPC, can be used in the future for such simulations.

1.4 High-order spectral methods

The advantage of the high-order spectral methods is that they avoid a large stencil, which is relevant for HPC. To compute the solution in the mesh cell, only information from neighbour elements are needed, so the stencil is the smallest possible. The idea of spectral technique is to consider the solution in each cell as a polynomial of degree p, given by $p+1$ coefficients in 1D while one DoF per cell is required with standard schemes. The procedure does not require a continuous solution at the mesh interface.

The high-order spectral methods can be classified in three groups: techniques which solve the weak (Discontinuous Galerkin - DG), the integral (Spectral Volume - SV) or the strong (Spectral Difference - SD, Flux Reconstruction - FR) form of the problem. Let give more details about these approaches:

1. The DG method combines elements from Finite Volume and Finite Element techniques. It is the oldest spectral approach introduced by Read and Hill in 1973 [25]. However, it was extended to full Navier-Stokes equations in 1997 by Bassi and Rabay [1]. Since the weak form of the equation is solved, it is mandatory to use complex integration rules to compute integrals of polynomials at a given order of accuracy. The recent Hybridized Discontinuous Galerkin method avoids this need for quadrature rules.

2. The SV technique is based on Finite Volume approach [31] and is not used any more.

3. The SD method joins elements from Finite Volume and Finite Difference techniques. It is stable and more CPU efficient than DG.

4. The FR approach appears first in 2007 [11]. It is similar to the SD, but uses a flux lifting operator (which is not unique) and accuracy, stability and FR properties depend on this

user-defined lifting operator. Moreover, it is weakly stable for certain configurations, but more CPU efficient than the DG, SV and SD methods.

Despite of the advantages of the high-order methods, they have also an important drawback, namely, their inability to handle flow discontinuities remains still a great challenge.

1.5 Presentation of the internship

This report follows 6 months of training period realized in the CFD aerodynamics team. More precisely, in a group composed of Jean-François Boussuge (project leader), Guillaume Puigt (senior researcher), Aravind Balan (postdoctoral researcher) and Julien Vanharen (PhD student).

The work is an extension of the report of Marie Lemesle [16] in which the analysis of several methods to handle flows with discontinuities is done for the hyperbolic problem of Burger's equation. Since this equation involves shock and rarefaction wave, it is a perfect test case to verify how different techniques capture and smooth numerical oscillations. The obtained results prove that the considered methods can be adapted to the SD approach and provide a good correction of non-regularity in the solution.

The goal in this internship is to analyze and to adapt to the Spectral Difference method some shock capturing techniques present in the literature. Some of them are implemented in JAGUAR - CERFACS in-house solver. The work is divided into several parts. At the beginning, the Spectral Difference approach is described in details for a hyperbolic problem and diffusion term. The isoparametric transformation is also introduced in order to diminish the computational cost of the solver. Afterwards, the standard test case of Sod's shock tube is presented and it is chosen to verify how well a code captures and resolves flow discontinuities. The approximated solution given by an initial version of JAGUAR (available at the beginning of the internship) is shown. Finally, techniques based on the artificial viscosity which enable to smooth spurious oscillations are described. For some of them, the approximated solution is presented and commented.

The current version of the report is considered to defend the Master of Sciences thesis but the internship is not finished. During the next three weeks, other test case will be analyzed and other method to treat flow discontinuities will be implemented in JAGUAR.

Chapter 2

Spectral Difference method

The Spectral Difference (SD) technique is a recent high-order approach which combines elements from Finite Volume (FV) and Finite Difference (FD) methods. Proposed by Kopriva and Kolias in 1995 [14] and 1996 [15] on quadrilateral structured meshes, this approach has been forgotten up to 2006 when Liu, Vinokur and Wang published a more general formulation on simplex elements [17, 18]. Finally, Wang, Liu and Sun extended it for 3D Navier-Stokes equations on hexahedral unstructured meshes in 2007 [28].

In this chapter, the Spectral Difference method is introduced in details. First, attention is focused on a hyperbolic problem in 1D. Then, the computation of diffusion term involving both solution and gradients is described. At the end, the key points to extend the approach to 2D and 3D flows by means of the isoparametric transformation are introduced. Finally, the global algorithm, as implemented in JAGUAR, is presented.

2.1 Details of the Spectral Difference approach in 1D

2.1.1 General principle

The following one-dimensional hyperbolic equation is considered in order to present details of the Spectral Difference (SD) method:

$$\frac{\partial Q}{\partial t} + \frac{\partial \mathcal{F}(Q)}{\partial x} = 0, \tag{2.1}$$

where Q is the unknown and $\mathcal{F}$ defines the flux (e.g. advection or convection flux). The domain is discretized by several 1D segments. The SD approach solves a strong form of the equation inside each mesh cell without needing for a continuous reconstruction of the solution at the cell boundary. Before entering into the details of the method, it is of great importance to introduce the general principles.

The basic principle of the SD method is to consider a solution Q as a polynomial of degree p in any segment and to solve Eq. 2.1 after projection onto the space of polynomials. If Q is a polynomial of degree p in space, its time derivative is also a polynomial of degree p. As a consequence and in order to be consistent with Eq. 2.1, the derivative of $\mathcal{F}$ must be a p-th order polynomial. Finally, by integration, the flux must be a polynomial of degree $p+1$ inside any cell. As a consequence, the SD method introduces a way to balance between two different polynomials for Q and $\mathcal{F}$, the flux polynomial being one degree higher than the solution polynomial. Finally, as soon as the value of $\frac{\partial \mathcal{F}}{\partial x}$ is known, the solution Q is computed

at the next time instant using a standard time integration algorithm such as a Runge-Kutta approach.

2.1.2 Description of the individual steps for a hyperbolic problem

In this section, explanations how the Spectral Difference method works in one-dimensional case are given. Knowing an approximate solution of the problem (2.1) at time t (or an initial solution at t_0), the objective is to find a solution after a time interval Δt.

Let consider a single mesh cell and the solution Q represented by a p-th order polynomial inside it. A p-th order polynomial is defined by its $p+1$ coefficients or conversely, by its value in $p+1$ different points. Instead of dealing with the polynomial coefficients, $p+1$ points where the solution is defined are introduced. They are called *Solution Points* (SP) and are noted $X_1, \ldots, X_{p+1}$.

As the solution at SP is known, using polynomial interpolation, the p-th order polynomial in the cell at fixed time t can be defined:

$$Q(x) = \sum_{i=1}^{p+1} Q(X_i) h_i(x), \tag{2.2}$$

where the set of functions $\{h_i(x) \mid i = 1, \ldots, p+1\}$ is the Lagrange basis:

$$h_i(x) = \prod_{s=1, s\neq i}^{p+1} \left(\frac{x - X_s}{X_i - X_s} \right) \quad \text{for} \quad i = 1, \ldots, p+1.$$

Let take an example of $p = 2$. In FIG. 2.1, the solution points, their associated solution and the second order interpolation polynomial are shown. Here, it is important to notice that SD approach is locally continuous but globally discontinuous.

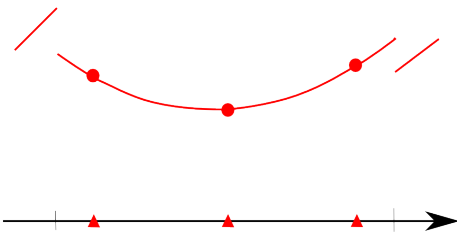

Figure 2.1: Step 0: Solution points (▲), solution (●) and 2^{nd} order interpolation polynomial in the cell

As the derivative of the flux $\mathcal{F}$ should be a polynomial of order p, the flux has to be of $(p+1)-th$ order. As for the solution, the flux polynomial is not defined by the $p+2$ polynomial coefficients, but from a set of $p+2$ values in points called *Flux Points* (FP). Let remark that the numbers of FP and SP differ by one and a 'natural' way to introduce the SP and FP follows a staggered way: a solution point is located between two flux points. The flux polynomial must be evaluated from the solution and the first step of the method is the extrapolation of the solution at the $p+2$ flux points. Since the approach is staggered, the FP are referred by $X_{1/2}, \ldots, X_{p+3/2}$, FIG. 2.2.

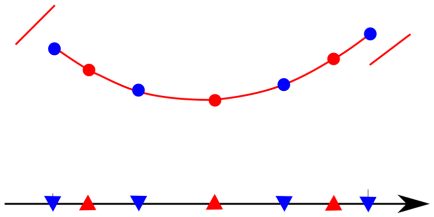

Figure 2.2: Step 1: Extrapolation of solution (•) at the flux points (▼)

At this moment, the flux $\mathcal{F}$ at flux points can be computed, Fig. 2.3. For example, for advection problem, the solution should be multiplied by the velocity. However, two different extrapolated quantities are obtained on the mesh interface. The solution at the interface being

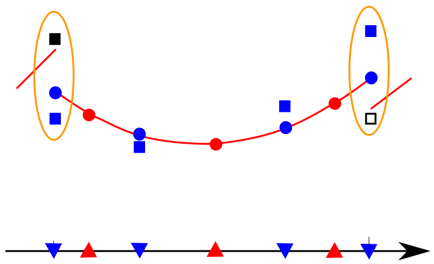

Figure 2.3: Step 2: Computing flux $\mathcal{F}$ (■) at flux points

discontinuous, it is typically a kind of Riemann's problem. The definition of the interface flux is unique and based on the application of an exact Riemann solver (Godunov's scheme) or an approximated Riemann solver (Roe's or Rusanov's schemes). The application of an upwind scheme drives two properties. First, the use of a Riemann solver guarantees conservation since the flux polynomial is continuous. Moreover, the upwind scheme is diffusive, which is a positive aspect for stability (Fig. 2.4).

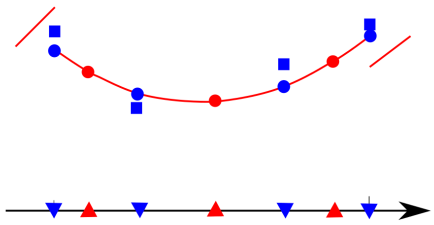

Figure 2.4: Step 3: Unique flux at interfaces thanks to Riemann solver

As before, using Lagrangian interpolation, a new $(p+1)-th$ order polynomial can be found from FP quantities:

$$\overline{\mathcal{F}}(Q(x)) = \sum_{i=0}^{p+1} \overline{\mathcal{F}}(Q(X_{i+1/2}))l_{i+1/2}(x), \tag{2.3}$$

where $\overline{\mathcal{F}}$ designates flux components such that the flux polynomial is made continuous across the mesh interfaces. The difference between $\mathcal{F}$ and $\overline{\mathcal{F}}$ lies on the definition of the flux at the cell interfaces. Moreover, the set of functions $\{l_{i+1/2}(x) \mid i = 0, \ldots, p+1\}$ is the Lagrange basis:

$$l_{i+1/2}(x) = \prod_{s=0, s\neq i}^{p+1} \left(\frac{x - X_{s+1/2}}{X_{i+1/2} - X_{s+1/2}} \right) \quad \text{for} \quad i = 0, \ldots, p+1.$$

This step of the method is represented in FIG. 2.5. Let remark that the constructed polynomial is globally continuous and differentiable inside each cell, but not at the interfaces.

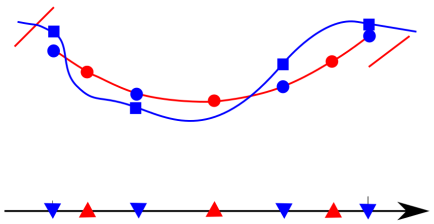

Figure 2.5: Step 4: $(p+1) - th$ order polynomial at flux points

Finally, a new flux polynomial (Eq. (2.3)) is differentiated at SP (FIG. 2.6):

$$\frac{\partial \overline{\mathcal{F}}(Q)}{\partial x}(X_s) = \sum_{i=0}^{p+1} \overline{\mathcal{F}}(Q(X_{i+1/2}))l'_{i+1/2}(X_s) \quad \text{for} \quad s = 1, \ldots, p+1.$$

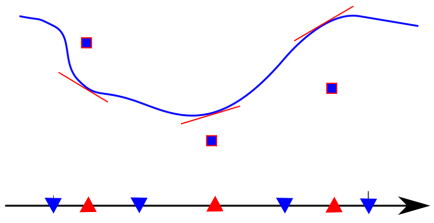

Figure 2.6: Step 5: Differentiation of the flux polynomial at solution points

At the end, the increment is computed thanks to the derivative of the flux at solution points and a time integration algorithm.

2.1.3 Description of the individual steps for the calculation of diffusion term

In the next chapters, some techniques to handle shocks which often require the computation of gradient or divergence are proposed. Moreover, the viscous flux of the Navier-Stokes equations demands the same work. Therefore, the solution gradients have to be calculated at flux points in order to compute a second-order derivative by differentiation. The method presented in this section is similar to the previous one and based on the extrapolation and the derivation.

But, in order to play with the Laplacian operator, it is mandatory to estimate the gradient polynomial at the same degree as the solution polynomial. Obtaining the p-th order gradient polynomial for a p-th order solution polynomial is the key point.

The first step of the method to compute a gradient is the same as before, *i.e.* the value Q_f at flux points from the solution Q at solution points is computed by interpolation, using Eq. 2.2 (FIG. 2.7).

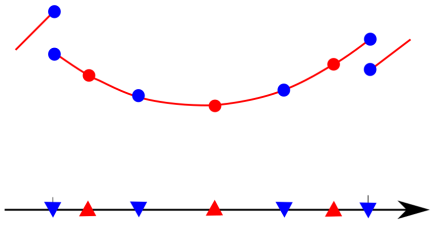

Figure 2.7: Step 1 : Extrapolation of solution (•) at flux points (▼)

This solution is again discontinuous at the interfaces. The interface quantity is then defined as the average of left and right contributions (centered scheme) as in [28] (Fig. 2.8).

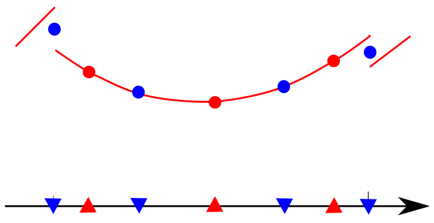

Figure 2.8: Step 2 : Computation of the average solution (•) at interfaces

A new interpolation polynomial is defined using $\overline{Q}_f$ at FP. Now, as previously, a polynomial is defined inside any mesh cell and it can be differentiated everywhere but the cell interfaces (FIG. 2.9). The next steps introduced in FIG. 2.10 and 2.11 consist in both the extrapolation

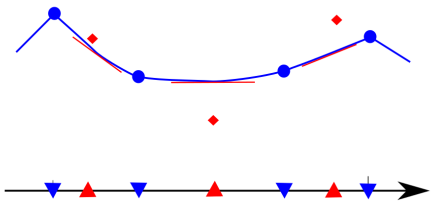

Figure 2.9: Step 3 : Construction of the continuous polynomial (blue) at flux points and derivation (♦) at solution points

of the gradient from SP to FP and the average of the solution gradient at the mesh interfaces. As before, it is a kind of centered scheme for the gradient.

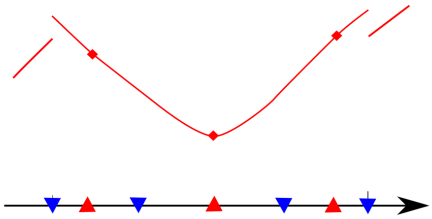

Figure 2.10: Step 4 : Definition of the derivative (red) at solution points

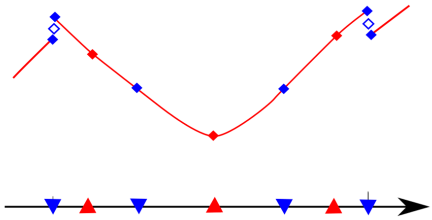

Figure 2.11: Step 5 : Extrapolation of the derivative (⧫) and computation of the continuous gradient at flux points

Finally, a continuous gradient polynomial $\overline{\nabla Q}_f$ at flux points is built and its divergence is computed to define the Laplacian operator.

2.2 Isoparametric transformation in 3D

The SD method is based on quadrilateral (in 2D) or hexahedral (in 3D) meshes. However, the shape of the cells changes if the mesh is not regular and as a consequence, the location of both SP as FP would change. In this context, the matrices introduced to perform extrapolation / interpolation and differentiation would be defined on a given cell. In order to minimize the data storage and help in the matrices definition for extrapolation and differentiation, an isoparametric transformation is introduced to convert any cell from the physical domain Ω_ϕ into the reference element $\Omega_{ref} = [0,1]^d$ (d is a space dimension). The goal is to solve the initial set of equations in the reference domain instead of the computational domain. The change of frame has an impact on the equations and in this section, details of the isoparametric transformation are described for 3D solutions.

To achieve an efficient implementation, all elements in the physical domain $(x, y, z) \in \Omega_\phi$ are transformed into a standard reference cell $(\xi, \eta, \psi) \in \Omega_{ref}$ using the following transformation:

$$\begin{pmatrix} x \\ y \\ z \end{pmatrix} = \sum_{i=1}^{K} M_i(\xi, \eta, \psi) \begin{pmatrix} x_i \\ y_i \\ z_i \end{pmatrix},$$

where K is the number of vertices used to define the physical element, (x_i, y_i, z_i) are Cartesian coordinates of those vertices, and $M_i(\xi, \eta, \psi)$ are the shape functions associated with the

isoparametric transformation.

Let consider the following hyperbolic equation in the physical domain:

$$\frac{\partial Q^{\phi}}{\partial t} + \frac{\partial f}{\partial x}(Q^{\phi}) + \frac{\partial g}{\partial y}(Q^{\phi}) + \frac{\partial h}{\partial z}(Q^{\phi}) = 0. \tag{2.4}$$

where Q^{ϕ} is the solution in the physical element and $\mathcal{F} = (f, g, h)^T$ designates a three-dimensional flux. Let convert Eq. 2.4 into the reference domain. Firstly, this equation can also be written as:

$$\begin{aligned}\frac{\partial Q^{\phi}}{\partial t} &+ \frac{\partial \xi}{\partial x}\frac{\partial f}{\partial \xi} + \frac{\partial \eta}{\partial x}\frac{\partial f}{\partial \eta} + \frac{\partial \psi}{\partial x}\frac{\partial f}{\partial \psi} + \\ &+ \frac{\partial \xi}{\partial y}\frac{\partial g}{\partial \xi} + \frac{\partial \eta}{\partial y}\frac{\partial g}{\partial \eta} + \frac{\partial \psi}{\partial y}\frac{\partial g}{\partial \psi} + \\ &+ \frac{\partial \xi}{\partial z}\frac{\partial h}{\partial \xi} + \frac{\partial \eta}{\partial z}\frac{\partial h}{\partial \eta} + \frac{\partial \psi}{\partial z}\frac{\partial h}{\partial \psi} = 0.\end{aligned}$$

Then, the solution in the physical domain Q^{ϕ} is transformed to the reference solution Q^{ref}:

$$Q^{ref} = |\mathcal{J}|Q^{\phi},$$

where $|\mathcal{J}|$ is the determinant of the Jacobian of the isoparametric transformation $\mathcal{J}$ defined as:

$$\mathcal{J} = \begin{pmatrix} \frac{\partial x}{\partial \xi} & \frac{\partial x}{\partial \eta} & \frac{\partial x}{\partial \psi} \\ \frac{\partial y}{\partial \xi} & \frac{\partial y}{\partial \eta} & \frac{\partial y}{\partial \psi} \\ \frac{\partial z}{\partial \xi} & \frac{\partial z}{\partial \eta} & \frac{\partial z}{\partial \psi} \end{pmatrix}.$$

If $|\mathcal{J}| \neq 0$ then the inverse transformation exists and its Jacobian matrix is given by

$$\mathcal{J}^{-1} = \begin{pmatrix} \frac{\partial \xi}{\partial x} & \frac{\partial \xi}{\partial y} & \frac{\partial \xi}{\partial z} \\ \frac{\partial \eta}{\partial x} & \frac{\partial \eta}{\partial y} & \frac{\partial \eta}{\partial z} \\ \frac{\partial \psi}{\partial x} & \frac{\partial \psi}{\partial y} & \frac{\partial \psi}{\partial z} \end{pmatrix}.$$

The equation becomes:

$$\begin{aligned}\frac{\partial Q^{ref}}{\partial t} + |\mathcal{J}| \Bigg(&\frac{\partial \xi}{\partial x}\frac{\partial f}{\partial \xi} + \frac{\partial \eta}{\partial x}\frac{\partial f}{\partial \eta} + \frac{\partial \psi}{\partial x}\frac{\partial f}{\partial \psi} + \\ &+ \frac{\partial \xi}{\partial y}\frac{\partial g}{\partial \xi} + \frac{\partial \eta}{\partial y}\frac{\partial g}{\partial \eta} + \frac{\partial \psi}{\partial y}\frac{\partial g}{\partial \psi} + \\ &+ \frac{\partial \xi}{\partial z}\frac{\partial h}{\partial \xi} + \frac{\partial \eta}{\partial z}\frac{\partial h}{\partial \eta} + \frac{\partial \psi}{\partial z}\frac{\partial h}{\partial \psi} \Bigg) = 0.\end{aligned}$$

Finally, the relationship between fluxes $(\tilde{f}, \tilde{g}, \tilde{h})^T$ in the reference domain and $(f, g, h)^T$ is the following one:

$$\begin{pmatrix} \tilde{f} \\ \tilde{g} \\ \tilde{h} \end{pmatrix} = |\mathcal{J}|\mathcal{J}^{-1} \begin{pmatrix} f \\ g \\ h \end{pmatrix}.$$

Then, the hyperbolic equation becomes:

$$\frac{\partial Q^{ref}}{\partial t} + \frac{\partial \tilde{f}}{\partial \xi}(Q^{ref}) + \frac{\partial \tilde{g}}{\partial \eta}(Q^{ref}) + \frac{\partial \tilde{h}}{\partial \psi}(Q^{ref}) = 0. \tag{2.5}$$

To conclude, Eq. (2.5) is always solved in the reference domain and a physical solution is only computed at the very end of the algorithm, essentially for visualization purpose.

2.3 Position of solution and flux points

The key point of the Spectral Difference method is the definition of solution and flux points in the reference element.

2.3.1 Definition in 1D

In our computations, the SP are chosen as Gauss-Lobatto points:

$$X_s = \frac{1}{2}\left[1 - \cos\left(\frac{2s-1}{2p+2}\pi\right)\right] \text{ with } s = 1, \ldots, p+1. \tag{2.6}$$

Remark: The SD method is not sensitive to the location of the SP and other choices are possible.

For the flux points position, a literature analysis shows that two set of positions are generally chosen. The first choice is the Gauss-Lobatto points:

$$X_{s+1/2} = \frac{1}{2}\left[1 - \cos\left(\frac{s}{p+1}\pi\right)\right] \text{ with } s = 0, \ldots, p+1.$$

However, Van den Abeele proved that this set of FP produces SD schemes unstable for $p > 2$ [30]. The other possibility is to select Legendre flux points, defined as the roots of Legendre polynomial of degree p shifted to the interval $[0, 1]$ plus the end points of the reference segment. The Legendre flux points are proven to be stable [12]. The Legendre flux points are the root of the Legendre polynomials and Legendre polynomials are a family of orthogonal polynomials defined as:

$$\frac{d}{dx}\left((1-x^2)P_n'(x)\right) + n(n+1)P_n(x) = 0, \quad P_n(1) = 1, \tag{2.7}$$

or by recurrence:

$$(n+1)P_{n+1}(x) = (2n+1)xP_n(x) - nP_{n-1}(x) \text{ with } P_0(x) = 1 \text{ and } P_1(x) = x.$$

It is also known that P_n is an $n-th$ order polynomial and has exactly n roots in the interval $]-1, 1[$.

To conclude this section, the standard SD approach demands a staggered mesh to find the solution, it means that between two solution points there is one flux point, which is verified by Gauss SP and Legendre FP, and which are considered during the internship.

2.3.2 Extension to 2D and 3D

Any quadrangle (or an hexahedron) defines 2 (resp. 3) privilegied space directions. The principle of the SD method is to keep the directional treatment on the reference element. From the solution at SP, the solution is extrapolated direction per direction to the flux points and the 1D procedure is applied direction per direction.

For a cell in dimension d, there are $(p+1)^d$ SP in the cell and $d(p+2)(p+1)^{d-1}$ FP in the element (or equivalently $(p+2)(p+1)^{d-1}$ per direction). The two sets of points in 2D are illustrated in FIG. 2.12.

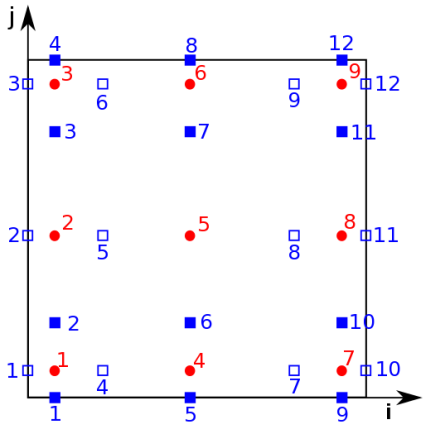

Figure 2.12: Position of solution and flux points for $p = 2$

2.4 Final algorithm in 3D for a hyperbolic problem

In summary, the algorithm to compute an approximate solution of the hyperbolic problem in 3D is based on several steps:

1. Define solution and flux points in the reference cell for a chosen polynomial degree p.
2. Initialize the solution in the physical domain.
3. Convert the physical solution Q^ϕ into the solution in the reference domain Q^{ref} at the solution points thanks to the formula: $Q^{ref} = |\mathcal{J}|Q^\phi$.

   At each time step:

4. Compute the extrapolated solution at flux points Q_f^{ref} using polynomial interpolation and known vector Q^{ref}:

$$Q_f^{ref}(\xi,\eta,\psi) = \sum_{k=1}^{p+1}\sum_{j=1}^{p+1}\sum_{i=1}^{p+1} Q_{i,j,k}^{ref} h_i(\xi)h_j(\eta)h_k(\psi),$$

   where $Q_{i,j,k}^{ref}$ is the solution at solution point (i,j,k) in the reference domain.

5. Transform the solution at flux points in the reference domain to the physical solution applying the relationship: $Q_f^{\phi} = \frac{Q_f^{ref}}{|\mathcal{J}|}$.

6. Calculate the flux $\overline{\mathcal{F}} = (\overline{f}, \overline{g}, \overline{h})^T$ in the physical domain:

   - at intern flux points directly applying the flux definition,
   - at interfaces using a Riemann solver.

7. Convert the flux $\overline{\mathcal{F}}$ into the flux in the reference domain $\tilde{\mathcal{F}} = (\tilde{f}, \tilde{g}, \tilde{h})^T$ with the expression: $\tilde{\mathcal{F}} = |\mathcal{J}|\mathcal{J}^{-1}\overline{\mathcal{F}}$.

8. Differentiate the flux polynomial (found using a Lagrangian interpolation) at solution points according to the formulas:

$$\frac{\partial \tilde{f}}{\partial \xi}(\xi,\eta,\psi) = \sum_{i=0}^{p+1}\sum_{j=1}^{p+1}\sum_{k=1}^{p+1} \tilde{f}_{i+1/2,j,k} l'_{i+1/2}(\xi) h_j(\eta) h_k(\psi),$$

$$\frac{\partial \tilde{g}}{\partial \eta}(\xi,\eta,\psi) = \sum_{i=1}^{p+1}\sum_{j=0}^{p+1}\sum_{k=1}^{p+1} \tilde{g}_{i,j+1/2,k} h_i(\xi) l'_{j+1/2}(\eta) h_k(\psi),$$

$$\frac{\partial \tilde{h}}{\partial \psi}(\xi,\eta,\psi) = \sum_{i=1}^{p+1}\sum_{j=1}^{p+1}\sum_{k=0}^{p+1} \tilde{h}_{i,j,k+1/2} h_i(\xi) h_j(\eta) l'_{k+1/2}(\psi).$$

9. Update the solution in the reference domain Q^{ref} thanks to the flux derivatives at solution points and time integration algorithm.

At the end, the final solution in the physical domain is obtained by applying $Q^{\phi} = \frac{Q^{ref}}{|\mathcal{J}|}$ at any point in the cell.

2.5 JAGUAR

JAGUAR (proJect of An Aerodynamic solver using General Unstructured grids And high ordeR schemes) is a new code developed by the CFD team at CERFACS. The project started in 2012 and the code is written in Fortran90.

The discretization technique implemented in JAGUAR is the Spectral Difference method. This choice was motivated by a few reasons. First, the formulation is simple, which leads to a straightforward implementation. Moreover, solving the strong form of the equation avoids the need for complex integration rules, as for integral-based approaches. Finally, the SD approach is known to be more CPU-efficient than the Discontinuous Galerkin method but a little bit less efficient than the Flux Reconstruction one.

JAGUAR solves 2D and 3D Euler and Navier-Stokes equations. JAGUAR handles High Performance Computing (HPC) capability and many efforts addressed this constraint. Several parallel paradigms are implemented, based on the standard libraries MPI[1], OpenMP[2] and hybrid (MPI and OpenMP).

[1] Message Passing Interface
[2] Open Multi-Processing

For the moment, only quadrilateral (in 2D) and hexahedral (in 3D) meshes are taken into account. The SD approach must be extended to any element shape but this is still a research domain. During this master thesis, efforts are dedicated to the implementation and validation of a shock capturing technique in order to deal with transonic and supersonic flows.

Chapter 3

Spectral Difference method and shocks

In this chapter, the definition of Euler equations necessary to describe the test case of shock tube, which is often considered to verify how well a code captures and resolves flow discontinuities, is recalled. For a given initial solution, its exact solution and the approximated solution given by the initial version of JAGUAR (available at the beginning of the internship) are presented. Finally, reasons why a shock capturing technique is mandatory to be added in JAGUAR are explained.

3.1 Sod's shock tube

The shock tube problem was introduced by Gary A. Sod in 1978 [27] in order to test the capability of various algorithms to solve fluid dynamics problems with shock wave behavior. This standard test case is very useful if shock capturing techniques are considered, because it involves the contact discontinuity, shock and rarefaction waves and its exact solution is known.

3.1.1 Euler equations in 3D

Euler equations of gas dynamics in 3D involve the following variables:

- ρ: the density (in $kg.m^{-3}$),
- $\vec{u}$: the velocity vector such as $\vec{u} = (u, v, w)^T$ (in $m.s^{-1}$),
- E: the total energy (in $m^2.s^{-2}$),
- p: the pressure (in Pa).

The total energy E is defined as:

$$E = e + \frac{\|u\|^2}{2},$$

where e represents the internal energy and the second term is the kinetic energy.

Finally, Euler equations in compact form are given by the following hyperbolic system:

$$\frac{\partial U}{\partial t} + \nabla \cdot F = 0, \tag{3.1}$$

where $U = (\rho, \rho u, \rho v, \rho w, \rho E)^T$ is the vector of conserved variables and $F = (F_1, F_2, F_3)$ is a three-dimensional flux whose components are defined as:

$$F_1 = \begin{pmatrix} \rho u \\ \rho u^2 + p \\ \rho uv \\ \rho uw \\ u(\rho E + p) \end{pmatrix}, \; F_2 = \begin{pmatrix} \rho v \\ \rho uv \\ \rho v^2 + p \\ \rho vw \\ v(\rho E + p) \end{pmatrix}, \; F_3 = \begin{pmatrix} \rho w \\ \rho uw \\ \rho vw \\ \rho w^2 + p \\ w(\rho E + p) \end{pmatrix}.$$

However, these five equations involve six unknowns, so it is mandatory to introduce other information to close the system. In the following, let suppose that

- the considered fluid verifies the ideal gas law:

  $$p = \rho RT,$$

  where T is the temperature (in K) and R is the specific gas constant (in $J.kg^{-1}.K^{-1}$),

- the gaz is polytropic, so characterized by the specific heat for a constant pressure C_p and the specific heat for a constant volume C_v given by

  $$C_p = \frac{\gamma R}{\gamma - 1}, \; C_v = \frac{R}{\gamma - 1},$$

  where γ is polytropic constant. Moreover, there is a linear relation between the internal energy and temperature:

  $$e = C_v T.$$

At this moment, the numbers of equations and unknowns are the same.

3.1.2 Description and exact solution of the shock tube

Let consider Euler equations of gas dynamics in 1D:

$$\frac{\partial S}{\partial t} + \frac{\partial W}{\partial x} = 0 \text{ for } t > 0, \; x \in \Omega, \tag{3.2}$$

where $S = (\rho, \rho u, \rho E)^T$, $W = (\rho u, \rho u^2 + p, u(\rho E + p))^T$ and $\Omega \subset \mathbb{R}$. Moreover, the initial solution is a Riemann problem given by:

$$S(t = 0, x) = \begin{cases} S_L & \text{if } x \leq x_0, \\ S_R & \text{if } x > x_0, \end{cases} \tag{3.3}$$

where $x_0 \in \mathbb{R}$ is an interface. Eq. (3.2) and (3.3) define the Sod's shock tube problem where x_0 can be seen as a diaphragm and S_L and S_R represent properties of the gas at the left and at the right of the interface. In the following, the gas is at rest in the whole domain and the pressure and the density are discontinuous across the interface:

$$S_L = \begin{pmatrix} \rho_L \\ u_L \\ p_L \end{pmatrix} = \begin{pmatrix} 1 \\ 0 \\ 1 \end{pmatrix}, \quad S_R = \begin{pmatrix} \rho_R \\ u_R \\ p_R \end{pmatrix} = \begin{pmatrix} 0.125 \\ 0 \\ 0.1 \end{pmatrix}.$$

As it exists a relation for perfect gases:

$$p = \rho(\gamma - 1)\left(E - \frac{1}{2}u^2\right),$$

the total energy can be found:

$$E_L = 2.5 \text{ and } E_R = 2.$$

Finally, Dirichlet boundary conditions are considered and the problem is well-posed. Due to the difference of the pressure and the density, the diaphragm is broken and three waves (rarefaction, shock, contact discontinuity) are created. The advantage of this test case is that its analytical solution can be computed [10, 20]. Details on the theoretical solution are introduced in Appendix A.

In the following, let $\Omega = [0, 1]$ and $x_0 = 0.5$. The exact solution of the shock tube problem at $t = 0.1$ is represented in Fig. 3.1. As mentioned before, three kinds of wave exist:

- the first one is a rarefaction wave between about $x = 0.38$ and $x = 0.5$,
- at about $x = 0.6$, the velocity and the pressure are continuous but the density is not, so it is a contact discontinuity,
- on the right, all variables are discontinuous, then there is a shock wave at about $x = 0.67$.

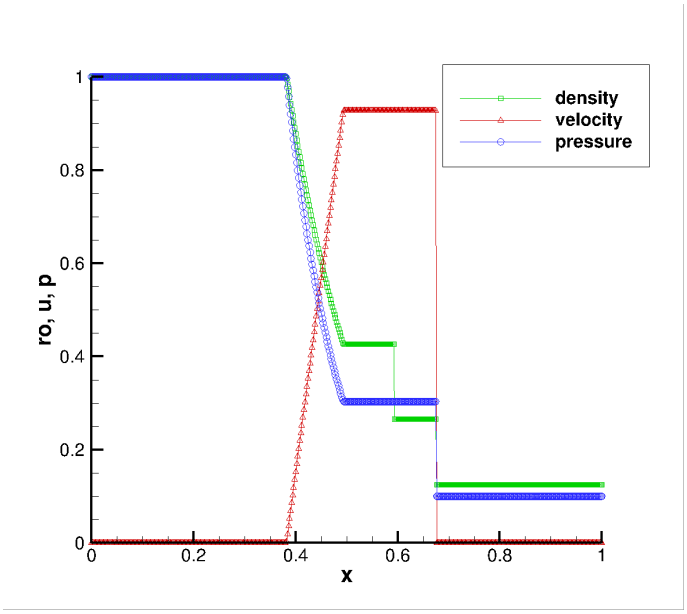

Figure 3.1: Sod's shock tube - exact solution at $t = 0.1$

3.1.3 Approximated solution - JAGUAR

Let take a look on the approximated solution given by JAGUAR with a basic Spectral Difference method. For a fair comparison, all computations are done with about 500 Degrees of

Freedom (DoF). Moreover, x_0 should not be in the middle of the cell due to the interpolation of the solution, which would create two artificial shocks at the end of the element including the interface. Therefore, x_0 is chosen to be between two cells. Details on the mesh definition are summarized in TAB. 3.1.

p	3	4	5
Number of cells	124	100	84
Number of DoF	496	500	504

Table 3.1: Details of the mesh used for further computation for each degree of polynomial p.

In FIG. 3.2-3.10, an approximated solution of a Sod's shock tube is represented. On the right of each figure, there is a zoom on the zone between the rarefaction and shock wave. For each polynomial order p, spurious oscillations appear in the solution. The smallest ones are near the head of the rarefaction and the highest next to the shock. Moreover, all region between these two waves is covered by oscillations, which increase a little bit for the density close to the contact discontinuity. However, there is no dependency between a polynomial order p and a size of oscillations.

3.2 Conclusion

Since the Spectral Difference method is based on the extrapolation and polynomial differentiation, it can not deal with flow discontinuities like shock wave or contact discontinuity. As shown in all figures from this chapter, solutions of problems involving any kind of discontinuities, such as shock tube, given by JAGUAR prove that numerical oscillations appear even near a rarefaction wave. Therefore, it is necessary to develop algorithms which are able to detect and correct the solution in every necessary zone. Then, it is mandatory to implement some of them in JAGUAR. In this work, several techniques based on the artificial viscosity to handle discontinuity are considered.

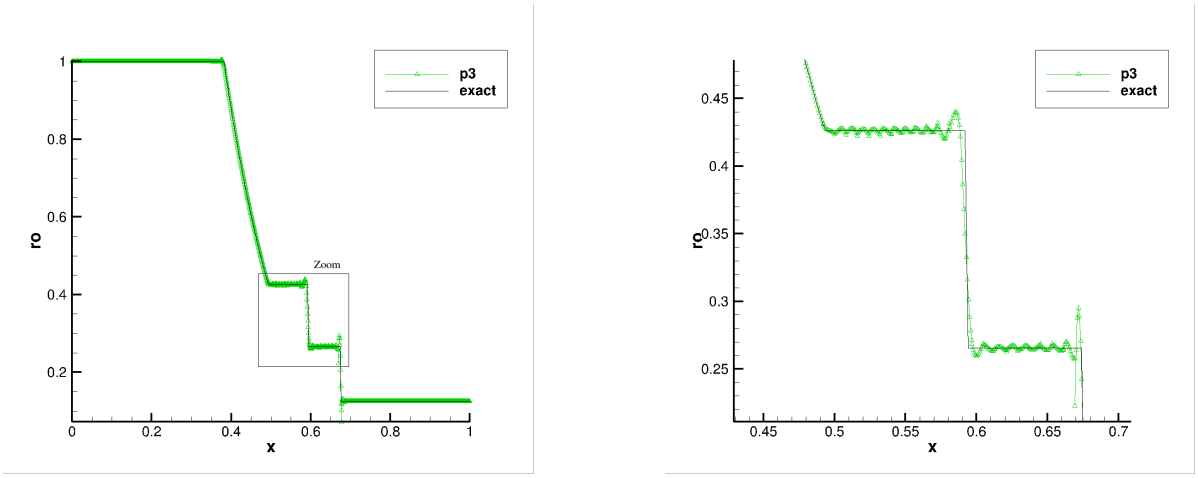

Figure 3.2: Density in the shock tube given by JAGUAR without any shock capturing technique for $p = 3$ at $t = 0.1$ (CFL=0.3, 496 DoF)

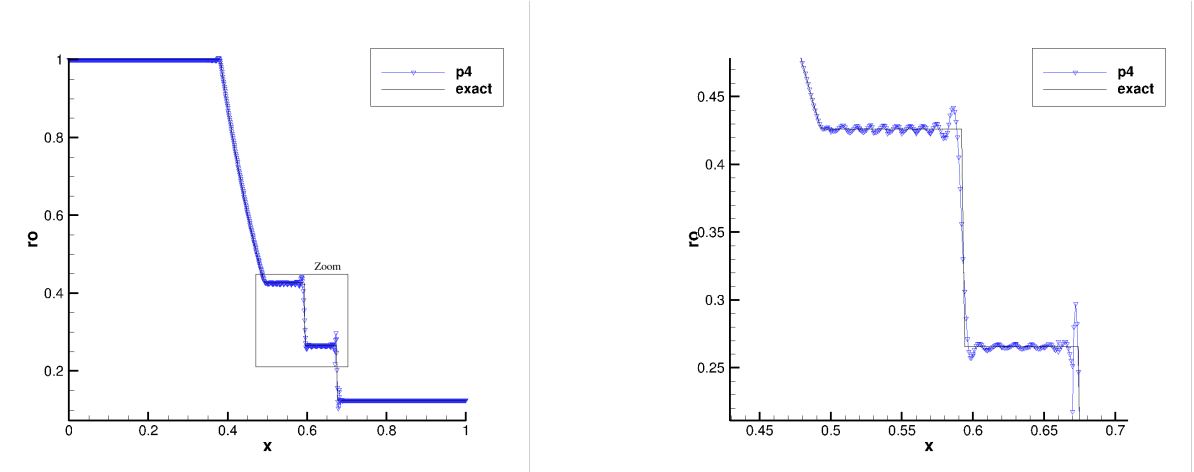

Figure 3.3: Density in the shock tube given by JAGUAR without any shock capturing technique for $p = 4$ at $t = 0.1$ (CFL=0.3, 500 DoF)

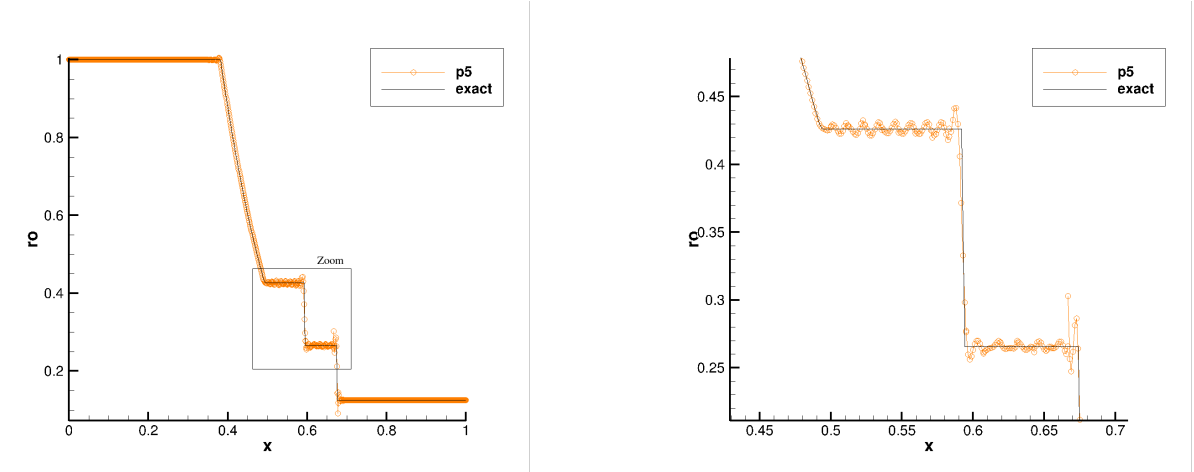

Figure 3.4: Density in the shock tube given by JAGUAR without any shock capturing technique for $p = 5$ at $t = 0.1$ (CFL=0.3, 504 DoF)

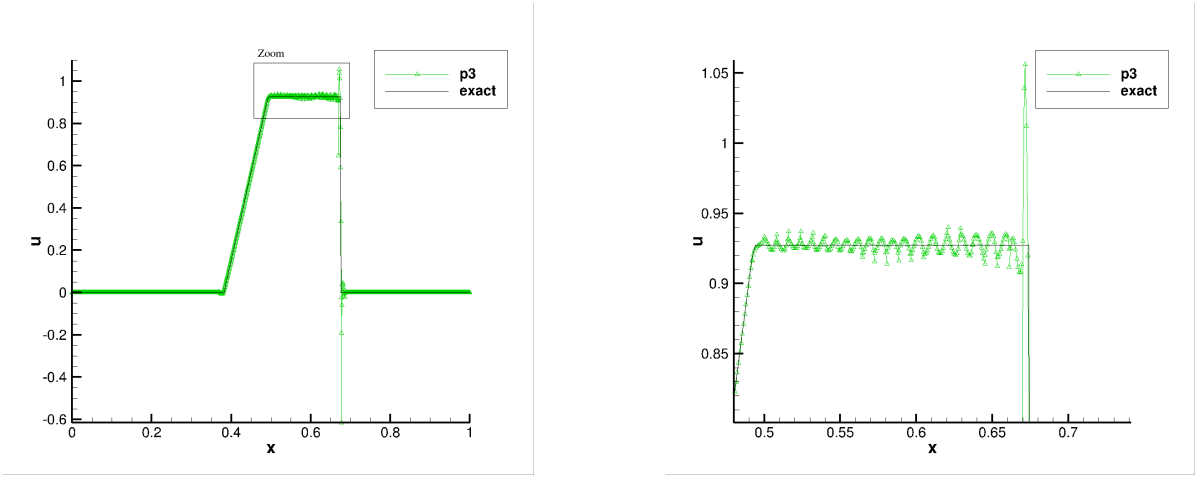

Figure 3.5: Velocity in the shock tube given by JAGUAR without any shock capturing technique for $p = 3$ at $t = 0.1$ (CFL=0.3, 496 DoF)

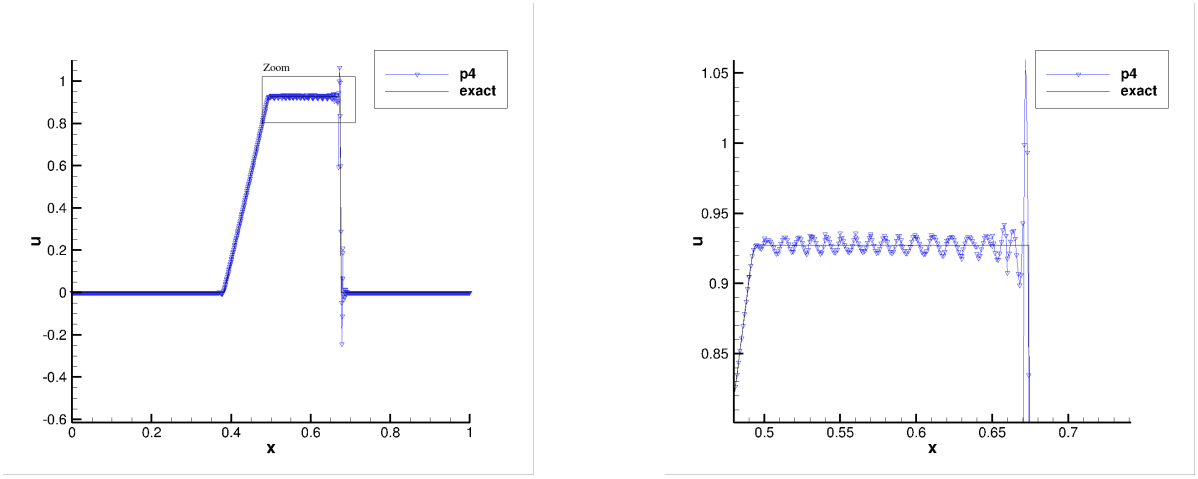

Figure 3.6: Velocity in the shock tube given by JAGUAR without any shock capturing technique for $p = 4$ at $t = 0.1$ (CFL=0.3, 500 DoF)

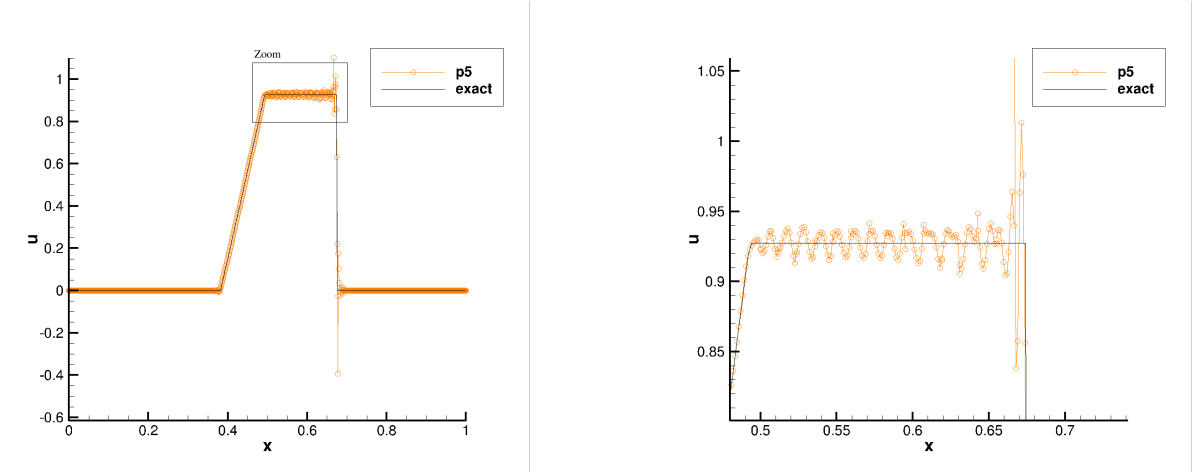

Figure 3.7: Velocity in the shock tube given by JAGUAR without any shock capturing technique for $p = 5$ at $t = 0.1$ (CFL=0.3, 504 DoF)

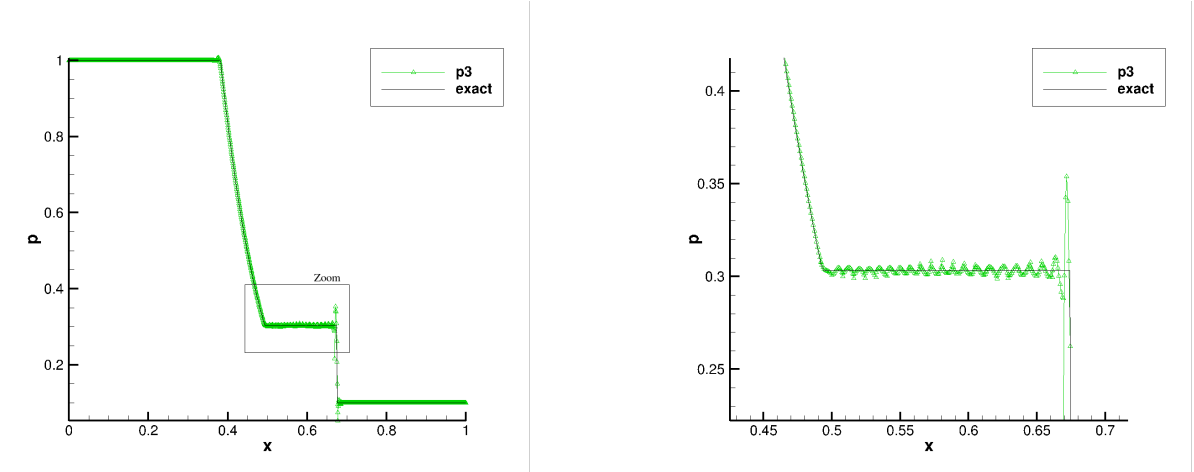

Figure 3.8: Pressure in the shock tube given by JAGUAR without any shock capturing technique for $p = 3$ at $t = 0.1$ (CFL=0.3, 496 DoF)

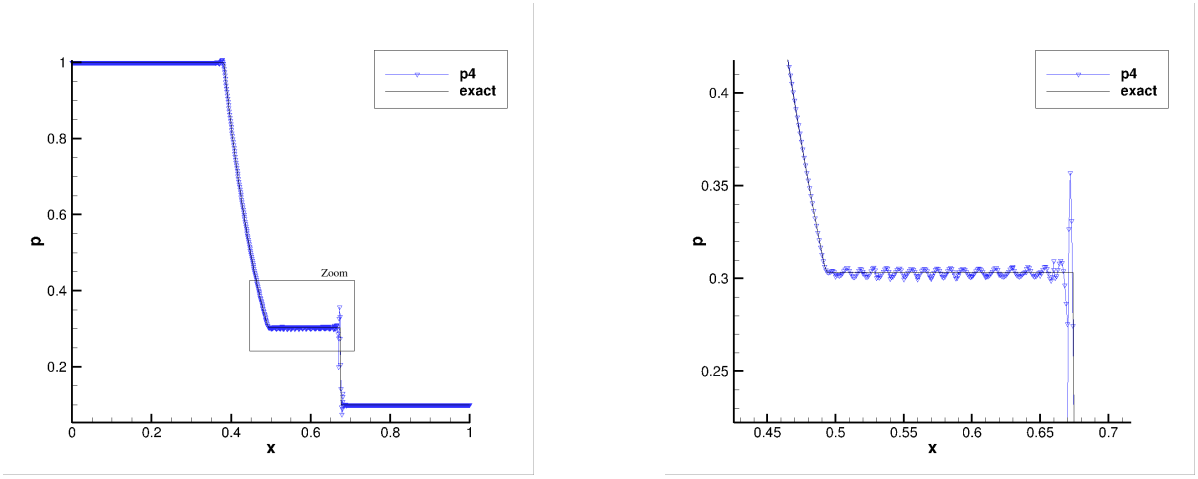

Figure 3.9: Pressure in the shock tube given by JAGUAR without any shock capturing technique for $p = 4$ at $t = 0.1$ (CFL=0.3, 500 DoF)

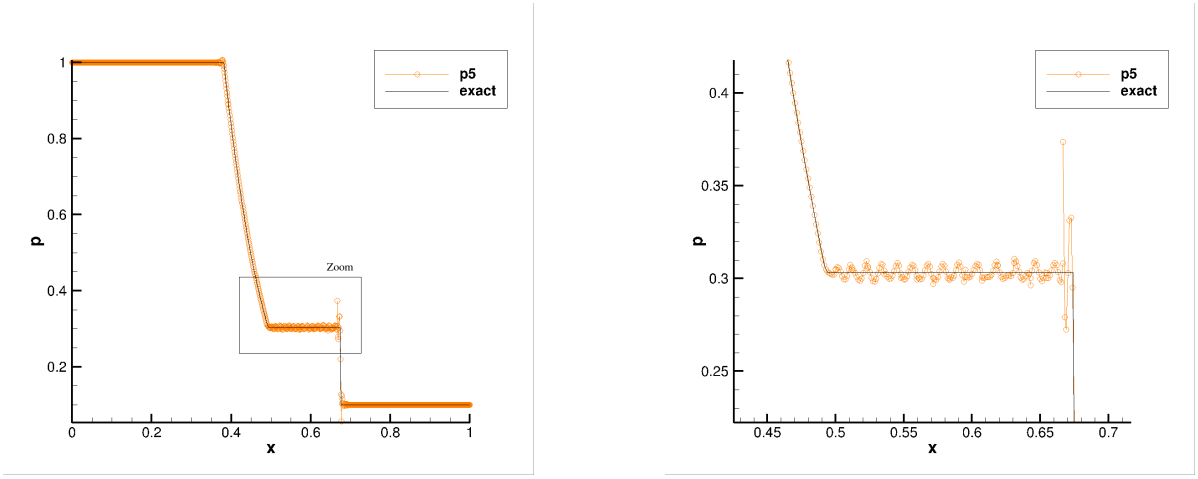

Figure 3.10: Pressure in the shock tube given by JAGUAR without any shock capturing technique for $p = 5$ at $t = 0.1$ (CFL=0.3, 504 DoF)

Chapter 4

Shock capturing techniques: constant viscosity

Many methods to deal with flow discontinuities can be found in the literature. The most known ones are: Linear Reconstruction [4, 32], Piecewise Parabolic Method (PPM) [29], Multi-dimensional Optimal Order Detection Method (MOOD) [3, 5, 6, 7, 21] and techniques based on the artificial viscosity, which are considered during the internship.

At the beginning of this chapter, the system of Euler equations with a smoothing operator is introduced. Then, the first and the simplest technique to handle shock based on the constant viscosity is presented.

4.1 Euler equations with a dissipation term

4.1.1 Extended Euler equations with a smoothing operator

Let consider a modified system of equations:

$$\frac{\partial U}{\partial t} + \nabla \cdot F = \varepsilon \, \Delta U, \tag{4.1}$$

where ε is a small amount of viscosity which is added in order to remove oscillations. This quantity can be defined in different ways as presented in the next sections. The idea of this approach is to solve Eq. (4.1) and consider this smooth solution as a solution of Euler equations.

4.1.2 Consequence on numerical algorithm

It is mandatory to add some steps to the basic algorithm described in the sec. 2.1.2 due to the dissipation term ΔU. Let recall that $\Delta U = \nabla \cdot \nabla U$ and that details to compute ∇U were presented in the sec. 2.1.3. The divergence of the gradient can be found in two steps. First, using the same algorithm as for ∇U, $\nabla (\nabla U)$ is computed and then it is simple to deduce $\nabla \cdot \nabla U$. Finally, ε should be defined.

4.2 Constant viscosity

4.2.1 Definition of the viscosity

The simplest choice is to suppose that the amount of viscosity is constant in the whole domain, so $\varepsilon = \varepsilon_0 \in \mathbb{R}^+$ and Eq. (4.1) becomes:

$$\frac{\partial U}{\partial t} + \nabla \cdot F = \varepsilon_0 \, \Delta U,$$

Let remark that if $\varepsilon_0 = 0$ then the basic equation (3.1) is solved. In fact, the higher quantity of viscosity is chosen, the smoother solution is obtained, so the aim of this method is to find ε_0 such as oscillations are removed but the accuracy is not affected too greatly.

4.2.2 Numerical results for Sod's shock tube

The results of the method for $p = 3, 4, 5$ with $\varepsilon_0 = 0.001$ can be seen in Fig. 4.1-4.3. On the right, there is a zoomed solution near the shock. All spurious oscillations are removed for the density and pressure. However, a little problem still remains for the velocity, but it is only visible with a zoom. Moreover, there is no special difference between solutions given by different polynomial degree.

Since the highest oscillations were located in the shock zone, a chosen quantity of the viscosity, necessary to smooth them all, is too large for other regions. For that reason, the rarefaction wave and the contact discontinuity are noticeably degraded.

4.2.2.1 Dependence of the CFL on the amount of the viscosity

As mentioned before, if ε_0 increases, the solution becomes smoother. But the solution can not be of high quality for large values of ε_0 since the solution is too much smoothed (Fig. 4.4). Moreover, for $\varepsilon_0 = 0.01$ and CFL$= 0.3$, the code crashes for $p = 3, 4, 5$. The following relation between the quantity of the viscosity and the stability condition is highlighted: the higher ε_0 and the higher polynomial degree p are, the smaller CFL has to be. Finally, in order to find the solution represented in Fig. 4.4, the corresponding stability condition taken is: for $p = 3, 4$ CFL $= 0.1$ and for $p = 5$ CFL $= 0.05$.

4.2.3 Conclusion

The main advantages of the method based on the constant artificial viscosity is the fact that it can remove all spurious oscillations and that it is very easy to implement. However, some important drawbacks should be mentioned. The value of ε_0 depends on the test case and it can be a complex task to find its proper value. Moreover, the main disadvantage is an addition of the artificial viscosity in the whole domain, which enables the loss of the accuracy in smooth regions, so it would be valuable to find a way to choose areas where some viscosity should be added. To do this, a *shock sensor* should be used. During the internship two sensors were considered [2, 8] and are described in details in Appendix B.

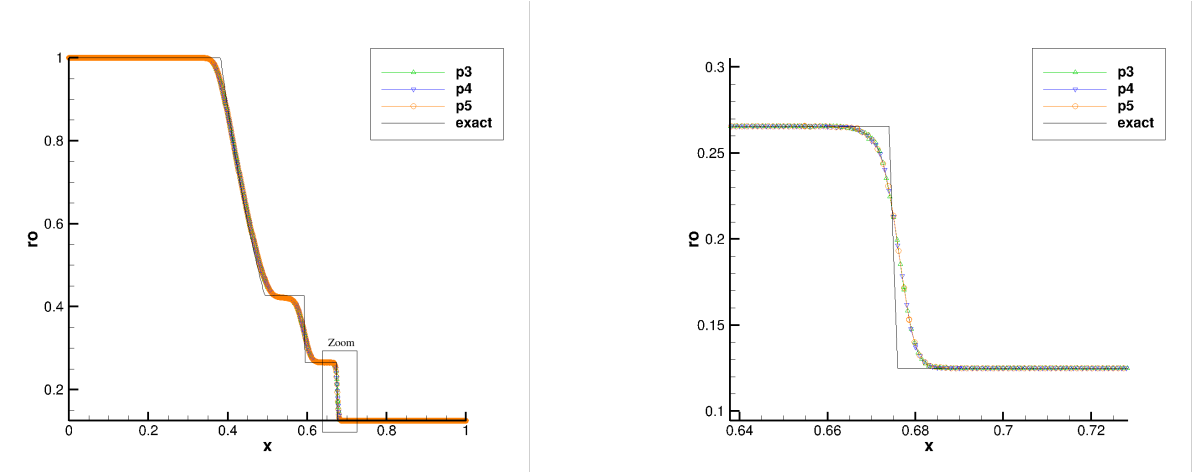

Figure 4.1: Density in the shock tube given by JAGUAR with the constant viscosity $\varepsilon_0 = 0.001$ for $p = 3, 4, 5$ at $t = 0.1$ (CFL=0.3, about 500 DoF)

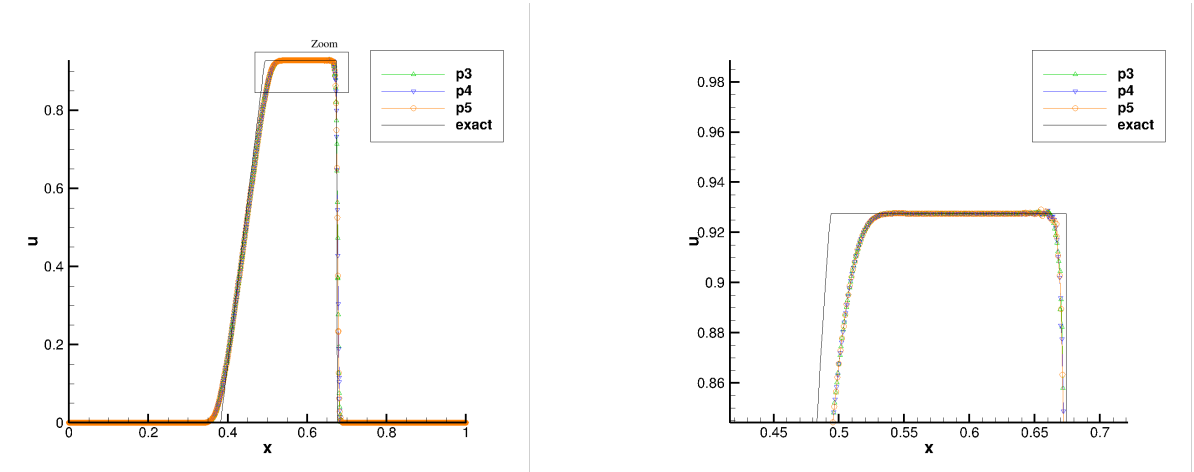

Figure 4.2: Velocity in the shock tube given by JAGUAR with the constant viscosity $\varepsilon_0 = 0.001$ for $p = 3, 4, 5$ at $t = 0.1$ (CFL=0.3, about 500 DoF)

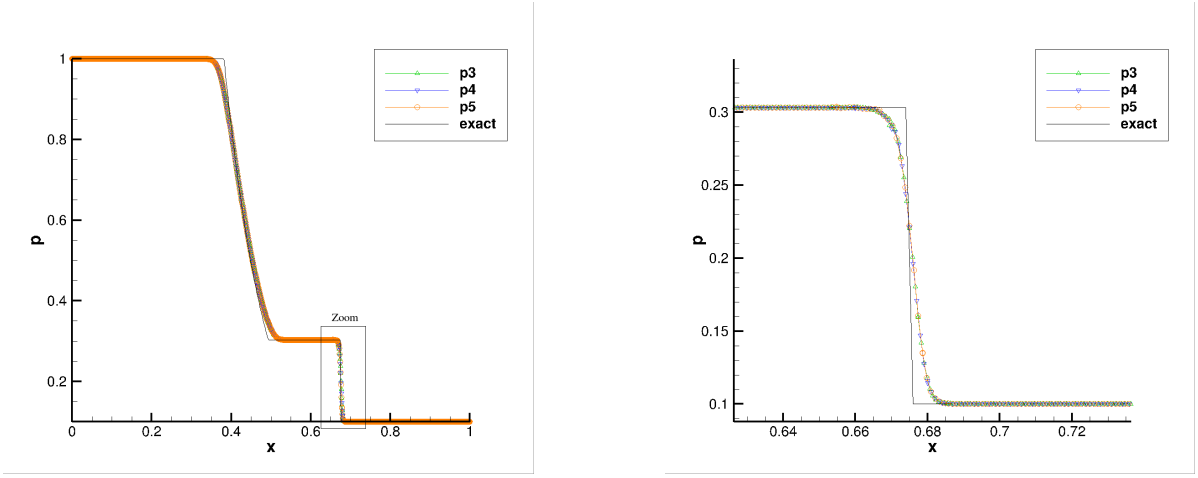

Figure 4.3: Pressure in the shock tube given by JAGUAR with the constant viscosity $\varepsilon_0 = 0.001$ for $p = 3, 4, 5$ at $t = 0.1$ (CFL=0.3, about 500 DoF)

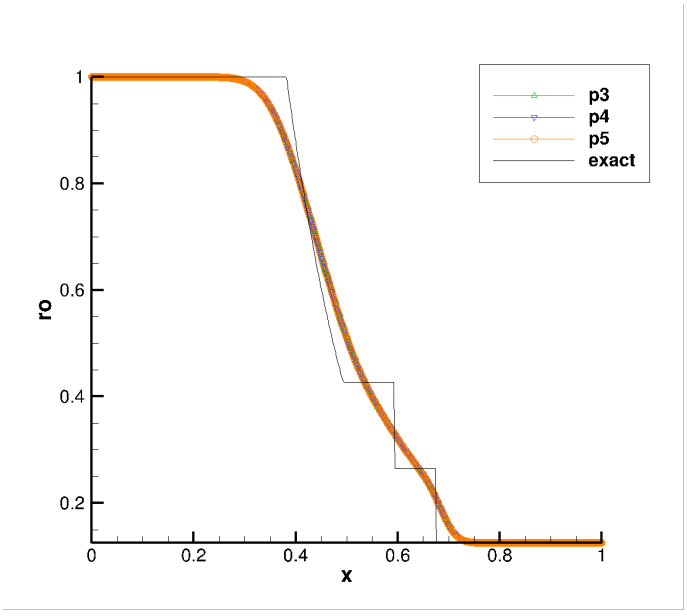

Figure 4.4: Density in the shock tube given by JAGUAR with the constant viscosity $\varepsilon_0 = 0.01$ for $p = 3$ (CFL=0.1), $p = 4$ (CFL=0.1) and $p = 5$ (CFL=0.05) at $t = 0.1$ and about 500 DoF

Chapter 5

Shock capturing techniques: localized Laplacian artificial viscosity

A new method to capture shocks, called Localized Laplacian Artificial Viscosity (LLAV), was proposed by Persson and Peraire in 2006 [24] for the Discontinuous Galerkin approach. Recently, Lodato adapted this technique to the SD framework [19].

The principle of LLAV is to construct a shock sensor based on the decay rate of the expansion coefficients of the solution in an orthogonal basis. For smooth solutions, the coefficients are expected to decay very quickly and for non-smooth solutions, rate of decay is dictated by the strength of the discontinuity. Then, this sensor is used to define the amount of the viscosity needed to remove oscillations.

5.1 New equation

The LLAV method is introduced using the following 1D equation:

$$\frac{\partial u}{\partial t} + \nabla \cdot f = \nabla \cdot (\varepsilon \, \nabla u) \,,$$

where u is the unknown, f defines the flux and ε is a function of viscosity computed in each cell as presented in the next section.

5.2 Definition of the viscosity

First, the solution u can be expressed in terms of the orthogonal basis as

$$u(x) = \sum_{i=1}^{N(p)} u_i \, \phi_i(x),$$

where $N(p)$ is the total number of terms in the expansion (in a directional approach: $N(p) = p + 1$) and $\{\phi_i \mid i = 1, \ldots, N(p)\}$ is a family of the orthogonal polynomials. Moreover, a truncated expansion of the same solution is considered:

$$\hat{u}(x) = \sum_{i=1}^{N(p-1)} u_i \, \phi_i(x).$$

Finally, the smoothness indicator is defined for each cell Ω_e:

$$S_e = \frac{(u-\hat{u}, u-\hat{u})_e}{(u,u)_e},$$

where $(\cdot,\cdot)_e$ is the standard inner product in $L_2(\Omega_e)$.

In the following, the orthonormal Legendre polynomials P_i^* are deduced from the orthogonal family P_i (introduced in the sec. 2.3) and are used as the definition of ϕ_i. Let recall the property of the Legendre polynomials:

$$\int_{-1}^{1} P_i(x)\, P_j(x)\, dx = \frac{2}{2i+1}\delta_{ij},$$

where δ_{ij} is the Kronecker symbol: $\delta_{ij} = \begin{cases} 1 & \text{if } i = j \\ 0 & \text{if } i \neq j \end{cases}$. So the orthonormal Legendre polynomial is given by

$$P_i^*(x) = P_i(x)\sqrt{\frac{2i+1}{2}}.$$

This choice of the orthogonal family enables to compute easily the sensor S_e. Actually:

$$u(x) = \sum_{i=1}^{N(p)} u_i^* P_{i-1}^*(x) \qquad \text{and} \qquad \hat{u}(x) = \sum_{i=1}^{N(p-1)} u_i^* P_{i-1}^*(x),$$

so:

$$(u-\hat{u}, u-\hat{u})_e = \int_{-1}^{1} \left(u_{p+1}^*\right)^2 P_p^*(x)\, P_p^*(x)\, dx = \left(u_{p+1}^*\right)^2$$

and

$$\begin{aligned}(u,u)_e &= \int_{-1}^{1} \sum_{i=1}^{N(p)} \sum_{j=1}^{N(p)} u_i^*\, u_j^*\, P_{i-1}^*(x)\, P_{j-1}^*(x)\, dx = \sum_{i=1}^{N(p)} \sum_{j=1}^{N(p)} u_i^*\, u_j^* \int_{-1}^{1} P_{i-1}^*(x)\, P_{j-1}^*(x)\, dx \\ &= \sum_{i=1}^{N(p)} \sum_{j=1}^{N(p)} \delta_{ij}\, u_i^*\, u_j^* = \sum_{i=1}^{N(p)} \left(u_i^*\right)^2.\end{aligned}$$

Once the value of the sensor is known, the constant diffusion coefficient is computed over each cell e by the following relation:

$$\varepsilon_e = \begin{cases} 0 & \text{if } s_e < s_0 - \kappa, \\ \frac{\varepsilon_0}{2}\left(1 + \sin\left(\frac{\pi(s_e - s_0)}{2\kappa}\right)\right) & \text{if } s_0 - \kappa \leq s_e \leq s_0 + \kappa, \\ \varepsilon_0 & \text{if } s_e > s_0 + \kappa, \end{cases} \tag{5.1}$$

where $s_e = \log_{10} S_e$, $\varepsilon_0 \approx h/p$ is the magnitude of the artificial viscosity (h is the size of the cell), $s_0 \approx 1/p^4$ and κ is chosen empirically sufficiently large so as to obtain a sharp but smooth shock profile. The final viscosity is a function of element-wise viscosity: $\varepsilon(x) = \varepsilon_{e(x)}$ where $e(x)$ designates the element to which x belongs.

5.2.1 Remarks

1. As the amount of the piecewise viscosity can vary a lot between two adjacent cells, it is beneficial to consider a version of $\varepsilon(x)$ with higher level of smoothness: $\varepsilon_0(x)$ for C^0-continuity or $\varepsilon_2(x)$ for C^2-continuity as proposed in [23].

2. The sensor S_e can robustly detect all kinds of flow discontinuities, but it can not distinguish its different types (e.g. shock and rarefaction waves). To diminish the amount of the viscosity near the expansion fan, Yu and Wang [33] proposed to correct the definition of ε_e according to the criterion: "if the velocity divergence $\nabla \cdot \vec{u}$ is larger than zero, then the flow field is treated as smooth". The new definition of the viscosity is:

$$\varepsilon_e^{corr} = \begin{cases} C_{div_u}\, \varepsilon_e & \text{if } \nabla \cdot \vec{u} > 0, \\ \varepsilon_e & \text{if } \nabla \cdot \vec{u} \leq 0, \end{cases}$$

   where C_{div_u} is a reduction parameter which should be set as 0. However, they find that a small value of C_{div_u} (e.g. $C_{div_u} \in [0.1, 0.3]$) can improve the results for some simulations.

3. According to Klöckner at al. [13], the estimation of s_0 in [23, 24] is wrong and to obtain a proper comparability, they take $s_0 \approx \log_{10}(1/p^4)$. In 2015, Yu [34] notes that s_0 should scale like $\log_{10}(1/p^3)$ in order to prevent the addition of the unnecessary numerical dissipation to relatively smooth flow features.

4. It is important not to set naively $\varepsilon_0 = h/p$, because the time-step size has to be (very often) significantly reduced to guarantee stability [22]. In the literature, we can find lots of definition of ε_0 [22, 33, 34].

5. In order to extend the method to higher dimensions, only the definitions of u and $\hat{u}$ change:

$$u(x,y,z) = \sum_{i=1}^{N(p)} \sum_{j=1}^{N(p)} \sum_{k=1}^{N(p)} u_{ijk}\, \phi_i(x)\, \phi_j(y)\, \phi_k(z),$$

$$\hat{u}(x,y,z) = \sum_{i=1}^{N(p-1)} \sum_{j=1}^{N(p-1)} \sum_{k=1}^{N(p-1)} u_{ijk}\, \phi_i(x)\, \phi_j(y)\, \phi_k(z).$$

5.3 Perspectives

During the internship, the LLAV method was implemented in JAGUAR. However, it is still in the phase of debugging. The last three weeks will be devoted to find bugs and proper parameters necessary to define the artificial viscosity for Sod's shock tube.

Chapter 6

Shock capturing techniques: concentration method

The concentration method presented in this chapter is based on the detection of jump discontinuities in piecewise smooth functions using their spectral data. Proposed by Gelb *et al.* in 1999 [9], it was extended by Sheshadri and Jameson in [26] to polynomial modes for the Discontinuous Galerkin technique and such an approach can be adapted for the Spectral Difference method.

At the beginning, the idea of the concentration method is described, then its extension in 1D and higher dimensions for SD technique is presented. Finally, numerical results for Sod's shock tube are commented.

6.1 Definition of the viscosity

6.1.1 Idea of the method

Let's note the jump at point x of the piecewise smooth function f with a single jump discontinuity by $[f](x) = f(x^+) - f(x^-)$, where x^+ (x^- resp.) denotes the right (left resp.) limit of f at x. Moreover, consider the *generalized conjugate Fourier partial sum* defined by:

$$\tilde{S}_N^\sigma[f](x) = \sum_{k=1}^{N} \sigma\left(\frac{k}{N}\right)(a_k \sin(kx) - b_k \cos(kx)),$$

where $\left(\hat{f}_k = a_k + ib_k\right)_{k=1}^{N}$ are the Fourier coefficients and $\sigma(\cdot)$ is called *concentration factor*. It is known that for $\sigma(x) \equiv 1$:

$$\frac{-\pi}{\log N}\, \tilde{S}_N^\sigma[f](x) \overset{N\to\infty}{\longrightarrow} [f](x)\, \delta_c(x),$$

where c is a point of discontinuity and $\delta_c(x) = \begin{cases} 1 & \text{if } x = c \\ 0 & \text{if } x \neq c \end{cases}$. Gelb and Tadmor in [9] extended this result and they obtained that

$$\tilde{S}_N^\sigma[f](x) \overset{N\to\infty}{\longrightarrow} [f](x)\, \delta_c(x)$$

for all nondecreasing $C^2[0,1]$ functions $\sigma(\cdot)$ which verify

$$\int_{1/N}^{1} \frac{\sigma(x)}{x}\, dx \overset{N\to\infty}{\longrightarrow} -\pi.$$

Finally, the idea of this method is to detect zones with discontinuity using the generalized conjugate Fourier partial sum, which can be seen as a sensor.

6.1.2 Principle for SD in 1D

The first step of the method consists of converting the nodal solution of a particular representative variable (called *density*) to modal one in each element e. The conversion is done by means of the matrix constructed by use of Legendre polynomials $\{P_i,\ i = 0, \dots, p\}$ evaluated at solution points:

$$\begin{pmatrix} \bar{f}_1 \\ \vdots \\ \bar{f}_{p+1} \end{pmatrix} = \begin{pmatrix} P_0(X_1) & \cdots & P_p(X_1) \\ \vdots & \ddots & \vdots \\ P_0(X_{p+1}) & \cdots & P_p(X_{p+1}) \end{pmatrix}^{-1} \begin{pmatrix} f_1 \\ \vdots \\ f_{p+1} \end{pmatrix},$$

where $(f_1, \dots, f_{p+1})^T$ is a nodal solution at SP and $(\bar{f}_1, \dots, \bar{f}_{p+1})^T$ represents a modal solution. Then, the identification of elements with discontinuity is done using the following sensor:

$$S_e = (p+1)^{r/2} \left| \max_{i=1,\dots,p+1} \left(\frac{\pi}{p+1} \sqrt{1 - X_i^2} \sum_{k=1}^{p+1} \sigma\left(\frac{|k|}{p+1} \right) \bar{f}_k P_k'(X_i) \right) \right|^r,$$

where $\sigma(\cdot)$ are concentration factors whose examples can be found in [9] and $r > 1$ is the enhancement exponent. Finally, if an element is identified as element with discontinuity, a technique to correct the solution should be applied. In this work, the definition of the artificial viscosity, proposed by Persson and Peraire [24] (Eq. (5.1)), is considered.

6.1.3 Extension to 2D and 3D

In this work, only quadrilateral and hexahedral meshes are considered. It means that each row and column of solution points in the element represents a 1D slice. The idea of the method is to apply the 1D concentration method to each slice in the cell and take as the value of the sensor the maximum value of sensors computed for each slice. Then, if necessary, the element is marked for special treatment.

6.2 Numerical results for Sod's shock tube

In Fig. 6.1-6.3, the numerical solutions given by JAGUAR with concentration method are presented for $p = 3, 4, 5$. As for the technique with the constant viscosity, a zoomed solution near the shock is on the right of each figure. All computations are done with $\sigma(x) \equiv 1$, $r = 3$, $\kappa = 4$, $s_0 = -3\log_{10}(p)$ and CFL $= 0.3$. However, the value of ε_0 changes with polynomial order p: $\varepsilon_0 = 0.003$ for $p = 3$, $\varepsilon_0 = 0.0045$ for $p = 4$ and $\varepsilon_0 = 0.0065$ for $p = 5$. The amount of the artificial viscosity is chosen in such a way that all spurious oscillations are removed from the pressure and the density. Three remarks can be done:

- The higher p is, the larger value of ε_0 has to be in order to smooth the solution.
- The higher oscillations are, the more important amount of viscosity should be applied to remove them all. For shock tube, the highest oscillations appear for the velocity near the shock and the value of ε_0 sufficient to correct the pressure and the density is not enough to smooth entirely the velocity (there is still a little problem visible on the zoom).

- As before, the rarefaction wave and the contact discontinuity are degraded.

6.3 Conclusion

The concentration method is considered as a first step to verify if there is no bug in the definition of the artificial viscosity implemented in JAGUAR for the LLAV technique.

Compared with the constant viscosity approach, this technique has a more complicated implementation. As shown in all figures from this chapter, the method gives a smooth solution without any oscillations, but the artificial viscosity is still added in smooth regions. In order to find a better solution, it would be valuable to do more tests with different parameters.

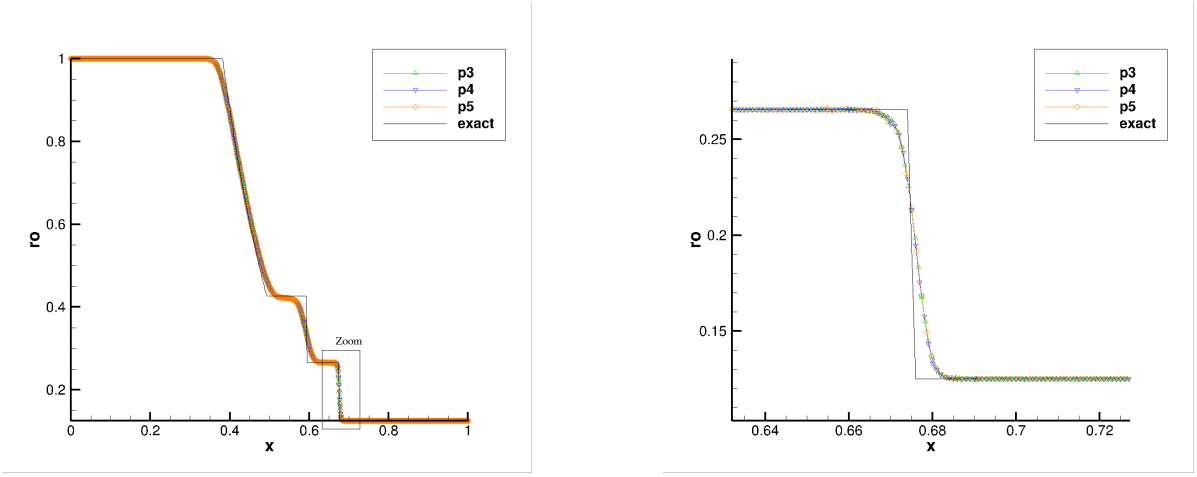

Figure 6.1: Density in the shock tube given by JAGUAR with the concentration method: $\varepsilon_0 = 0.003$ for $p = 3$, $\varepsilon_0 = 0.0045$ for $p = 4$ and $\varepsilon_0 = 0.0065$ for $p = 5$ at $t = 0.1$ ($\sigma(x) \equiv 1$, $r = 3$, $\kappa = 4$, $s_0 = -3\log_{10}(p)$, CFL=0.3, about 500 DoF)

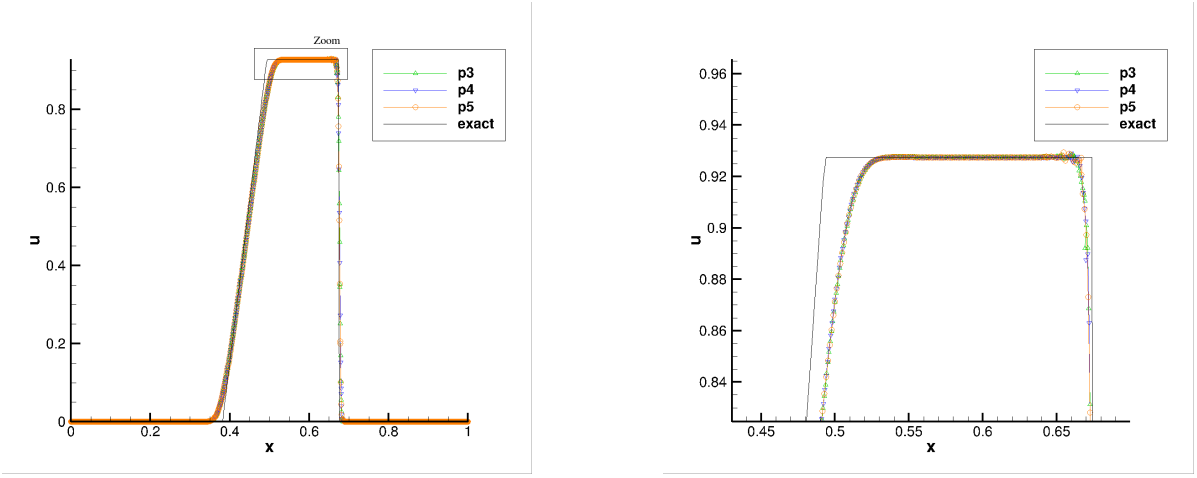

Figure 6.2: Velocity in the shock tube given by JAGUAR with the concentration method: $\varepsilon_0 = 0.003$ for $p = 3$, $\varepsilon_0 = 0.0045$ for $p = 4$ and $\varepsilon_0 = 0.0065$ for $p = 5$ at $t = 0.1$ ($\sigma(x) \equiv 1$, $r = 3$, $\kappa = 4$, $s_0 = -3\log_{10}(p)$, CFL=0.3, about 500 DoF)

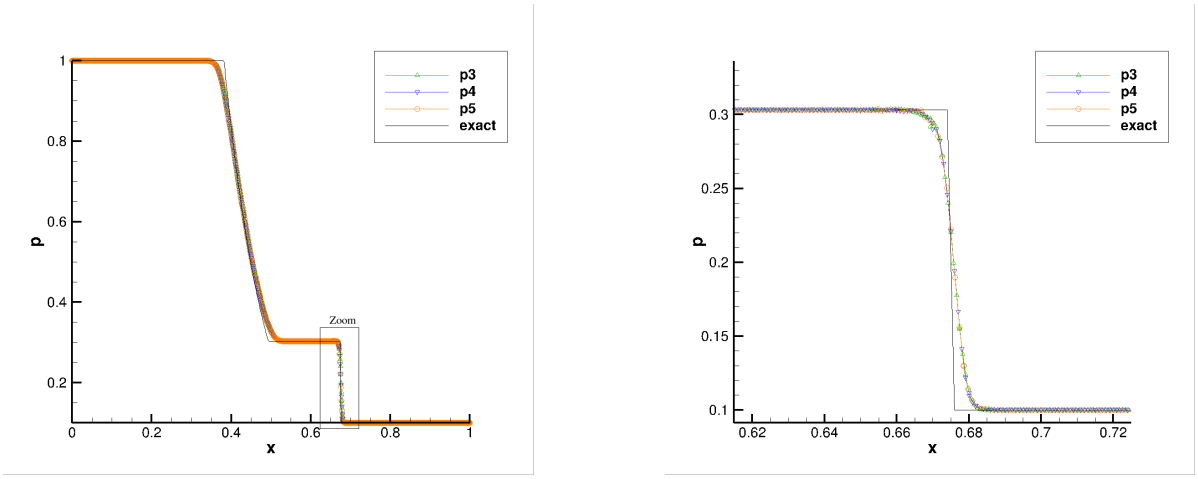

Figure 6.3: Pressure in the shock tube given by JAGUAR with the concentration method: $\varepsilon_0 = 0.003$ for $p = 3$, $\varepsilon_0 = 0.0045$ for $p = 4$ and $\varepsilon_0 = 0.0065$ for $p = 5$ at $t = 0.1$ ($\sigma(x) \equiv 1$, $r = 3$, $\kappa = 4$, $s_0 = -3\log_{10}(p)$, CFL=0.3, about 500 DoF)

Chapter 7

Comparison of the constant viscosity and concentration method

In this chapter, the numerical results for the method based on the constant artificial viscosity and the concentration technique are compared.

Let recall all parameters used for computations. All simulations are stopped at $t = 0.1$ and CFL $= 0.3$ is considered. Moreover, for the concentration method $\sigma(x) \equiv 1$, $r = 3$, $\kappa = 4$ and $s_0 = -3\log_{10}(p)$. Finally, the amount of the artificial viscosity necessary to find a smooth solution is detailed in Tab. 7.1.

polynomial degree p	3	4	5
ε_0 for the constant viscosity	0.001	0.001	0.001
ε_0 for the concentration method	0.003	0.0045	0.0065

Table 7.1: Details of the amount of the artificial viscosity for each degree of polynomial p used for computations.

The approximated solution found for these parameters is represented in Fig. 7.1-7.9. Three points can be highlighted:

1. The two techniques gives a regular and similar solution, however they degrade a lot smooth regions.
2. For a given polynomial order p, the amount of viscosity necessary to remove oscillations is higher for the concentration method than for the constant viscosity.
3. The concentration approach gives a slightly better solution than other technique, especially near the rarefaction wave.

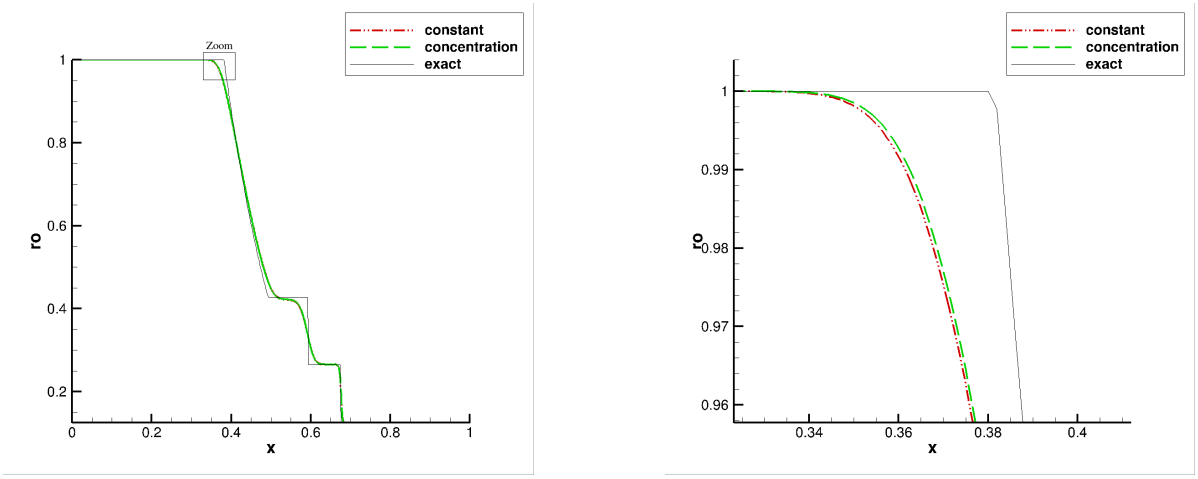

Figure 7.1: Density in the shock tube given by JAGUAR with the constant viscosity $\varepsilon_0 = 0.001$ and concentration method with $\varepsilon_0 = 0.003$, $\sigma(x) \equiv 1$, $r = 3$, $\kappa = 4$ and $s_0 = -3\log_{10}(p)$ for $p = 3$ at $t = 0.1$ (CFL=0.3, about 500 DoF)

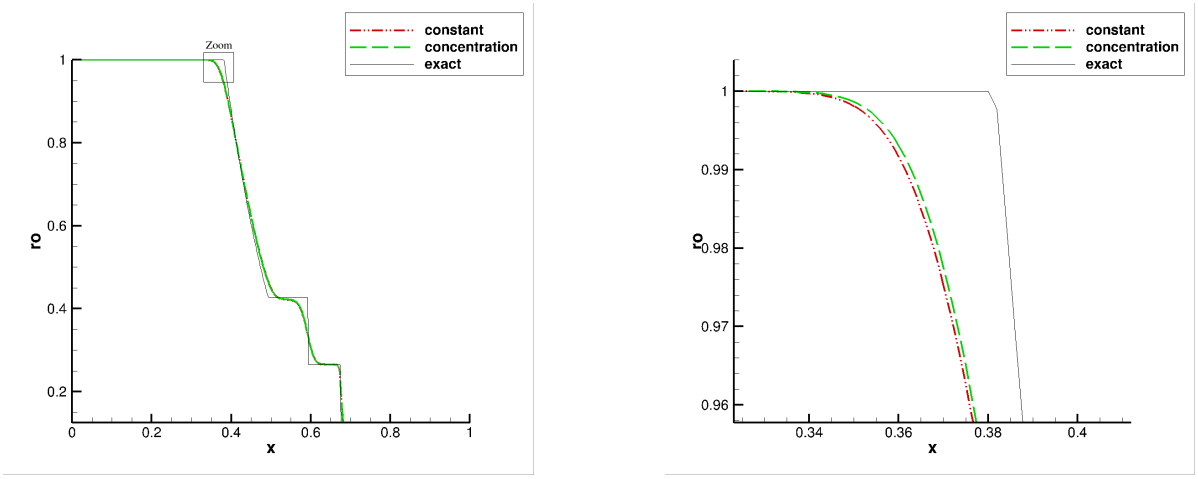

Figure 7.2: Density in the shock tube given by JAGUAR with the constant viscosity $\varepsilon_0 = 0.001$ and concentration method with $\varepsilon_0 = 0.0045$, $\sigma(x) \equiv 1$, $r = 3$, $\kappa = 4$ and $s_0 = -3\log_{10}(p)$ for $p = 4$ at $t = 0.1$ (CFL=0.3, about 500 DoF)

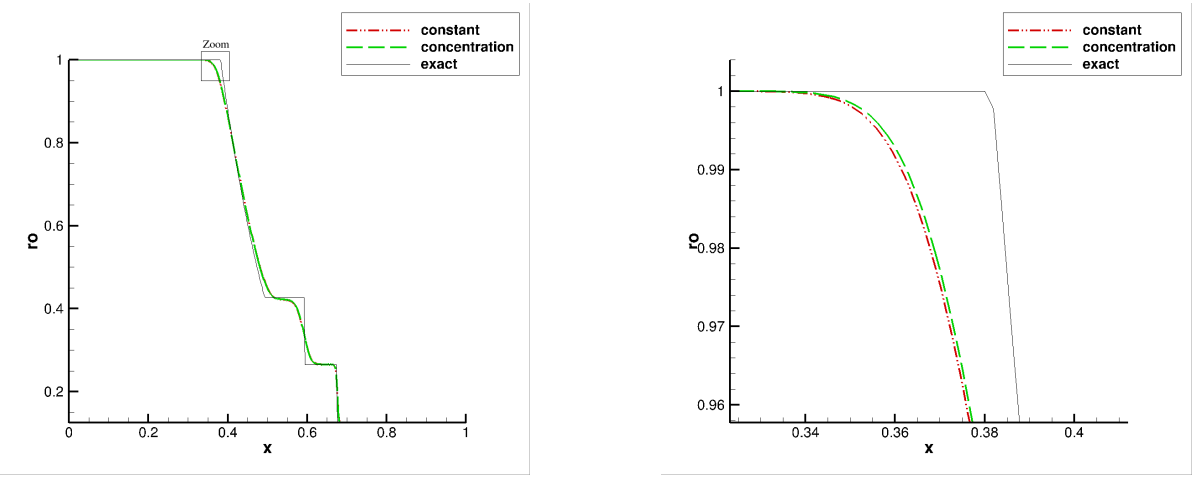

Figure 7.3: Density in the shock tube given by JAGUAR with the constant viscosity $\varepsilon_0 = 0.001$ and concentration method with $\varepsilon_0 = 0.0065$, $\sigma(x) \equiv 1$, $r = 3$, $\kappa = 4$ and $s_0 = -3\log_{10}(p)$ for $p = 5$ at $t = 0.1$ (CFL=0.3, about 500 DoF)

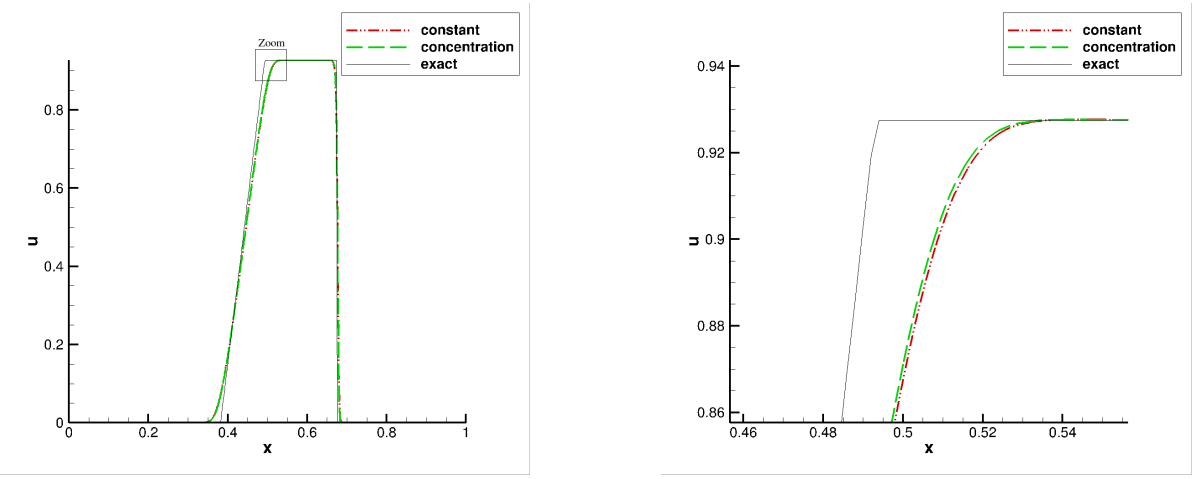

Figure 7.4: Velocity in the shock tube given by JAGUAR with the constant viscosity $\varepsilon_0 = 0.001$ and concentration method with $\varepsilon_0 = 0.003$, $\sigma(x) \equiv 1$, $r = 3$, $\kappa = 4$ and $s_0 = -3\log_{10}(p)$ for $p = 3$ at $t = 0.1$ (CFL=0.3, about 500 DoF)

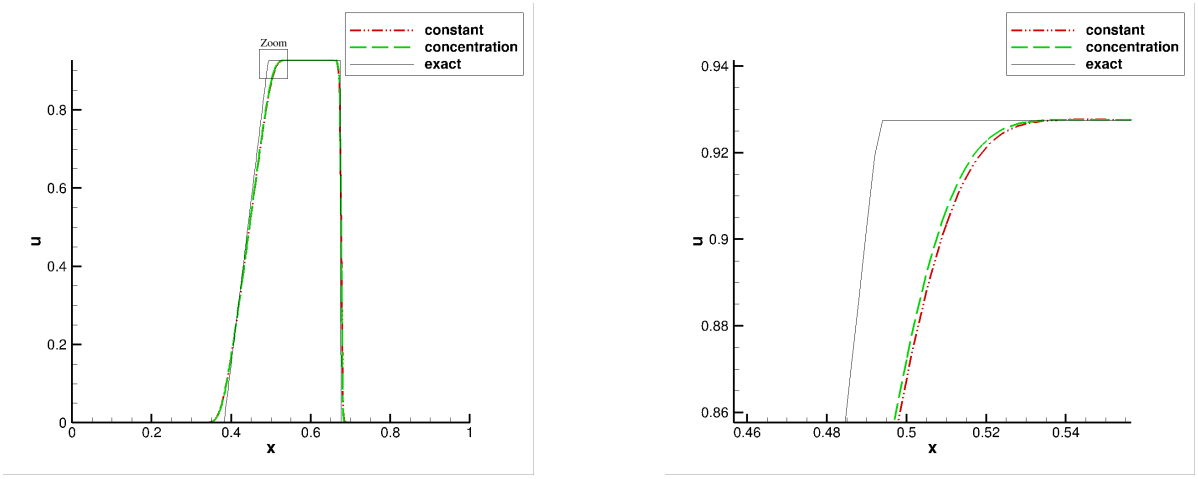

Figure 7.5: Velocity in the shock tube given by JAGUAR with the constant viscosity $\varepsilon_0 = 0.001$ and concentration method with $\varepsilon_0 = 0.0045$, $\sigma(x) \equiv 1$, $r = 3$, $\kappa = 4$ and $s_0 = -3\log_{10}(p)$ for $p = 4$ at $t = 0.1$ (CFL=0.3, about 500 DoF)

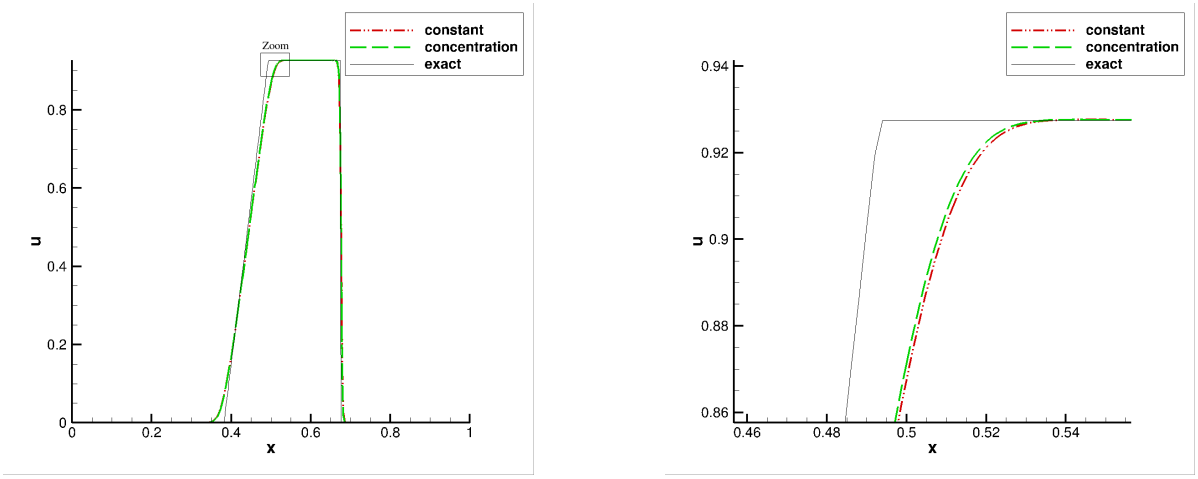

Figure 7.6: Velocity in the shock tube given by JAGUAR with the constant viscosity $\varepsilon_0 = 0.001$ and concentration method with $\varepsilon_0 = 0.0065$, $\sigma(x) \equiv 1$, $r = 3$, $\kappa = 4$ and $s_0 = -3\log_{10}(p)$ for $p = 5$ at $t = 0.1$ (CFL=0.3, about 500 DoF)

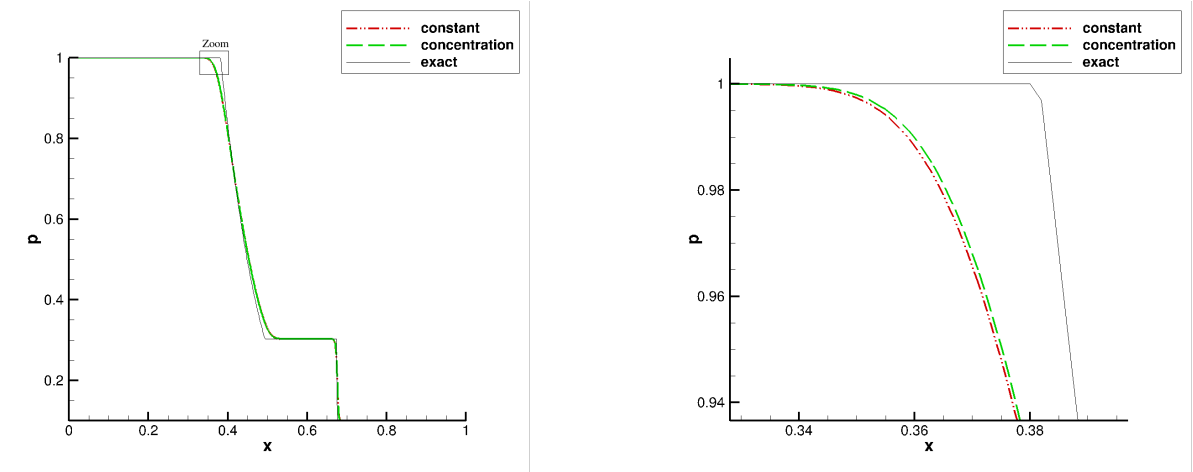

Figure 7.7: Pressure in the shock tube given by JAGUAR with the constant viscosity $\varepsilon_0 = 0.001$ and concentration method with $\varepsilon_0 = 0.003$, $\sigma(x) \equiv 1$, $r = 3$, $\kappa = 4$ and $s_0 = -3\log_{10}(p)$ for $p = 3$ at $t = 0.1$ (CFL=0.3, about 500 DoF)

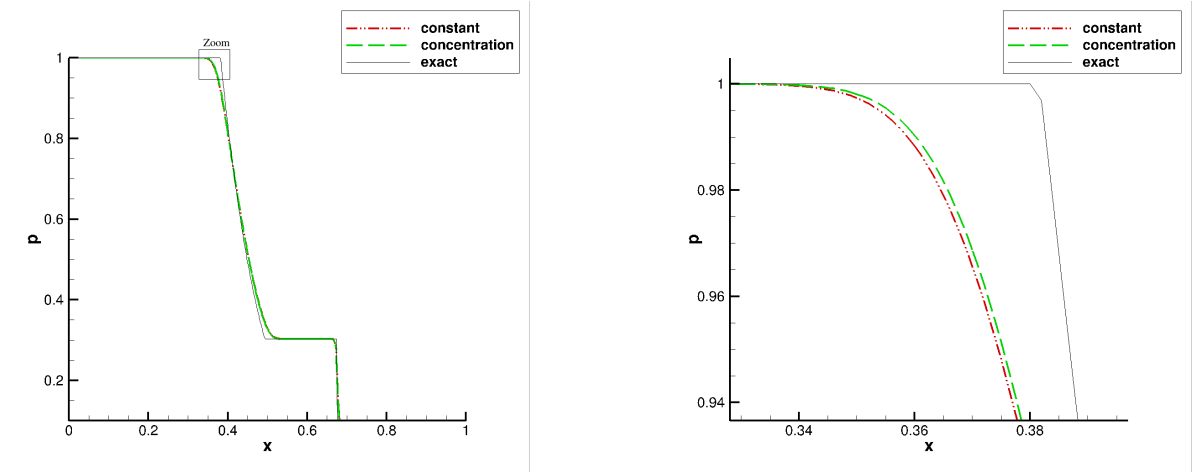

Figure 7.8: Pressure in the shock tube given by JAGUAR with the constant viscosity $\varepsilon_0 = 0.001$ and concentration method with $\varepsilon_0 = 0.0045$, $\sigma(x) \equiv 1$, $r = 3$, $\kappa = 4$ and $s_0 = -3\log_{10}(p)$ for $p = 4$ at $t = 0.1$ (CFL=0.3, about 500 DoF)

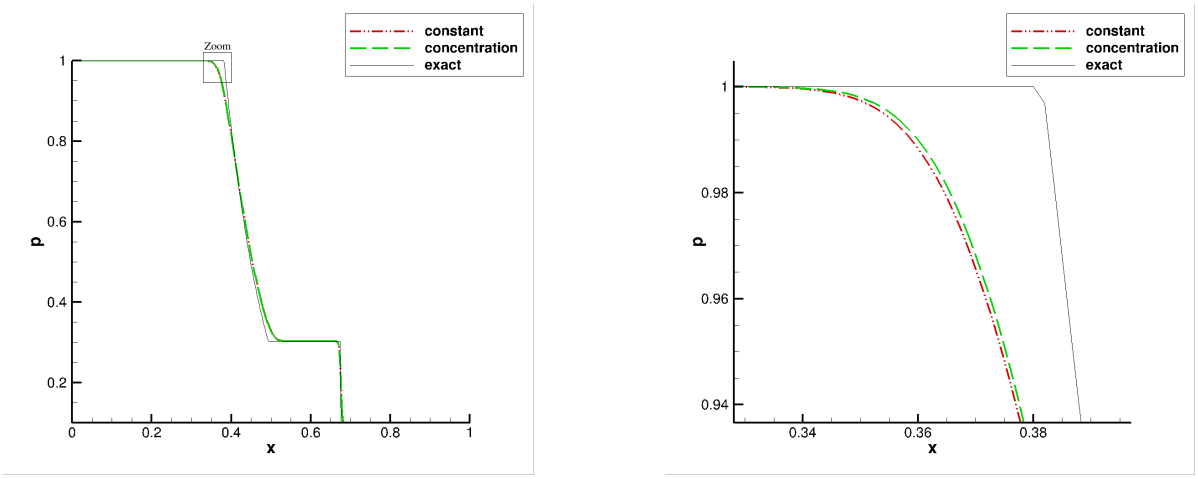

Figure 7.9: Pressure in the shock tube given by JAGUAR with the constant viscosity $\varepsilon_0 = 0.001$ and concentration method with $\varepsilon_0 = 0.0065$, $\sigma(x) \equiv 1$, $r = 3$, $\kappa = 4$ and $s_0 = -3\log_{10}(p)$ for $p = 5$ at $t = 0.1$ (CFL=0.3, about 500 DoF)

Chapter 8

Conclusion and perspectives

This Master of Science thesis treats the extension of the Spectral Difference solver JAGUAR to handle discontinuous flows. JAGUAR is a new CFD code solving the Euler and Navier-Stokes equations using the Spectral Difference method which belongs to the family of high-order discontinuous spectral techniques and which does not deal itself with shocks.

The idea of the Spectral Difference approach is to represent the solution as a polynomial inside each mesh cell and it is based mainly on the extrapolation and polynomial differentiation. Since the method is only locally continuous, in order to deal with discontinuities at the interfaces a Riemann solver is used for a hyperbolic problem and a centered scheme for a diffusion term. Moreover, the isoparametric transformation is applied in order to cast the initial problem into a reference domain.

The Sod's shock tube was considered as a test case to show that for each order of accuracy of the method, the approximated solution given by an initial version of JAGUAR without shock treatment includes spurious oscillations. Moreover, they are present not only near the shock wave but also near the rarefaction wave and the contact discontinuity. However, there is no special difference between a chosen polynomial degree and the size of oscillations.

All methods implemented in JAGUAR during the internship are based on the artificial viscosity. It means that instead of looking for the solution of the basic problem, Euler equations with a smoothing operator are solved. Among techniques available in the literature, three of them were chosen: constant viscosity, localized Laplacian artificial viscosity and concentration method. They were adapted to the Spectral Difference approach and implemented in the code.

The first and the simplest technique considered was the method based on the constant artificial viscosity. It is simple to implement and enables to remove all spurious oscillations from the solution. However, the smoothing operator is applied in the whole domain even in regions where it is not necessary. For this reason, the rarefaction wave and the contact discontinuity are visibly degraded. To overcome this effect, it would be valuable to implement a sensor whose aim is to detect zones with non-regularity.

The second technique which was chosen is localized Laplacian artificial viscosity proposed by Persson and Peraire for the Discontinuous Galerkin method. This approach includes computation of the sensor which enables to eliminate numerical oscillations without degrading smooth areas of the solution. For now, the technique is in the phase of debugging. However, G. Lodato adapted and successfully implemented this method in his Spectral Difference solver.

The last technique is the concentration method which is similar to the previous one and it was possibly to verify if the definition of the viscosity is well implemented for it. The solution obtained for the shock tube proves that the technique removes all oscillations, but the rarefaction wave and contact discontinuity are still too much smoothed. However, this method

is slightly better than the constant viscosity, because it degrades less the solution in regular areas.

The internship will be finished on September 30th and during the next three weeks the localized Laplacian artificial viscosity method will be analyzed in order to find why it does not work. Moreover, standard transonic test cases will be considered to verify if all implemented techniques gives a desirable solution. Finally, if solutions are convincing, it is planned to extend the results presented in the report to prepare an article to submit to a refereed journal.

APPENDIX A: Analytical solution of Sod's shock tube

In this chapter, the following system of equations is considered:

$$\frac{\partial S}{\partial t} + \frac{\partial W}{\partial x} = 0 \text{ for } t > 0,\ x \in \mathbb{R}, \tag{A.1}$$

where $S = (\rho, \rho u, \rho E)^T$ and $W = (\rho u, \rho u^2 + p, u(\rho E + p))^T$. Let recall also a relation for perfect gases:

$$p = \rho(\gamma - 1)\left(E - \frac{1}{2}u^2\right),\ E = e + \frac{1}{2}u^2. \tag{A.2}$$

Moreover, the initial data of a Riemann problem is given by:

$$S(t = 0, x) = \begin{cases} S_L & \text{if } x \leq x_0, \\ S_R & \text{if } x > x_0, \end{cases}$$

with S_L and S_R which represent properties of the gas at the left and at the right from an interface x_0.

First step: Determine the matrix $A(S')$ such as:

$$\frac{\partial S'}{\partial t} + A(S')\frac{\partial S'}{\partial x} = 0 \text{ for } t > 0,\ x \in \mathbb{R},$$

where $S' = (\rho, u, p)^T$ is a vector of primitive variables.

The first equation of the system (A.1) implies:

$$\frac{\partial \rho}{\partial t} + \frac{\partial(\rho u)}{\partial x} = 0 \Leftrightarrow \frac{\partial \rho}{\partial t} + u\frac{\partial \rho}{\partial x} + \rho\frac{\partial u}{\partial x} = 0. \tag{A.3}$$

In the following, let suppose that $\rho \neq 0$ and using Eq. (A.3), the second line of $A(S')$ can be found:

$$\frac{\partial(\rho u)}{\partial t} + \frac{\partial(\rho u^2 + p)}{\partial x} = 0 \Leftrightarrow u\frac{\partial \rho}{\partial t} + \rho\frac{\partial u}{\partial t} + u\frac{\partial(\rho u)}{\partial x} + \rho u\frac{\partial u}{\partial x} + \frac{\partial p}{\partial x} = 0 \Leftrightarrow$$

$$\frac{\partial u}{\partial t} + u\frac{\partial u}{\partial x} + \frac{1}{\rho}\frac{\partial p}{\partial x} = 0. \tag{A.4}$$

Finally, the last equation is considered and by means of Eq. (A.2) and (A.4), the third line is deduced:

$$\frac{\partial(\rho E)}{\partial t} + \frac{\partial(u(\rho E + p))}{\partial x} = 0 \Leftrightarrow \frac{\partial\left(\rho e + \frac{1}{2}\rho u^2\right)}{\partial t} + \frac{\partial\left(\rho u e + \frac{1}{2}\rho u^3 + up\right)}{\partial x} = 0 \Leftrightarrow$$

$$\frac{\partial p}{\partial t} + \gamma p \frac{\partial u}{\partial x} + u \frac{\partial p}{\partial x} = 0.$$

Then, the matrix $A(S')$ is:

$$A(S') = \begin{pmatrix} u & \rho & 0 \\ 0 & u & \frac{1}{\rho} \\ 0 & \gamma p & u \end{pmatrix}.$$

Second step: Determine the eigenvalues of $A(S')$.

Let solve the equation $\det(A(S') - \lambda I) = 0$:

$$\det \begin{pmatrix} u-\lambda & \rho & 0 \\ 0 & u-\lambda & \frac{1}{\rho} \\ 0 & \gamma p & u-\lambda \end{pmatrix} = (u-\lambda)\left(u - \lambda - \sqrt{\frac{\gamma p}{\rho}}\right)\left(u - \lambda + \sqrt{\frac{\gamma p}{\rho}}\right).$$

So, $\det(A(S') - \lambda I) = 0 \Leftrightarrow \lambda \in \{u - c, u, u + c\}$, where $c = \sqrt{\frac{\gamma p}{\rho}}$.

Third step: Determine the eigenvectors of $A(S')$ (see Tab. A.1).

eigenvalue	eigenvector
$u - c$	$\left(1,\ \frac{-c}{\rho},\ c^2\right)^T$
u	$(0,\ 1,\ 0)^T$
$u + c$	$\left(1,\ \frac{c}{\rho},\ c^2\right)^T$

Table A.1: Eigenvalues and eigenvectors of the matrix $A(S')$.

It is easy to check that these pairs verify: $A(S')r = \lambda r$, where r is an eigenvector corresponding to the eigenvalue λ.

Fourth step: Determine the nature of waves (see Tab. A.2).

Conclusion: The final solution of a Riemann problem (A.1) is composed of four possibilities:

1. rarefaction wave + contact discontinuity + rarefaction wave,
2. rarefaction wave + contact discontinuity + shock wave,
3. shock wave + contact discontinuity + rarefaction wave,
4. shock wave + contact discontinuity + shock wave.

λ	$\nabla_{S'}\lambda$	r	$\nabla_{S'}\lambda \cdot r$	nature
$u-c$	$\left(\frac{1}{2}\sqrt{\frac{\gamma p}{\rho^3}},\ 1,\ -\frac{1}{2}\sqrt{\frac{\gamma}{\rho p}}\right)^T$	$\left(1,\ \frac{-c}{\rho},\ c^2\right)^T$	$\neq 0$	GNL
u	$(0,\ 1,\ 0)^T$	$(1,\ 0,\ 0)^T$	0	LD
$u+c$	$\left(-\frac{1}{2}\sqrt{\frac{\gamma p}{\rho^3}},\ 1,\ \frac{1}{2}\sqrt{\frac{\gamma}{\rho p}}\right)^T$	$\left(1,\ \frac{c}{\rho},\ c^2\right)^T$	$\neq 0$	GNL

Table A.2: Verification of the nature of waves (LD - linearly degenerate, GNL - genuinely non-linear)

In the following, only the case 2 is considered. It corresponds to a standard shock tube (i.e. higher density and pressure at the left from an interface, and the velocity is set to zero in the whole domain). The exact solution without details is presented (see [20] for computations for all combinations of waves).

The solution is studied in five regions which are represented on the FIG. A.1. Let start

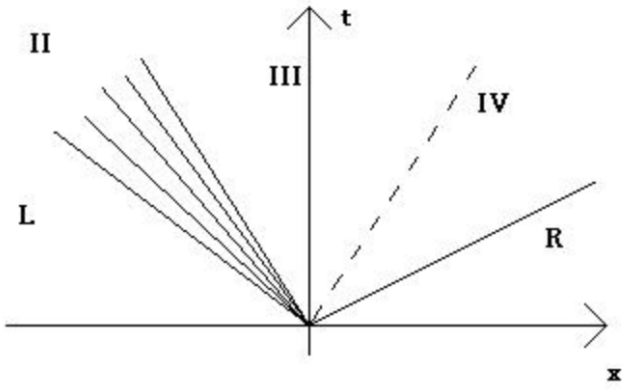

Figure A.1: Description of regions for Sod's shock tube

with two regions next to the contact discontinuity. The theoretical analysis implies that the pressure and velocity are constant across them. Moreover, the velocity in the third region is given by:

$$v_3 = v_L - \frac{2c_L}{\gamma - 1}\left(\left(\frac{p_3}{p_L}\right)^{\frac{\gamma-1}{2\gamma}} - 1\right),$$

and in the fourth one by:

$$v_4 = v_R + (p_4 - p_R)\sqrt{\frac{A_R}{p_4 + B_R}},$$

where $A_R = \frac{2}{(\gamma+1)\rho_R}$ and $B_R = \frac{\gamma-1}{\gamma+1}p_R$. Now, using relations: $v_3 = v_4$ and $p_3 = p_4$ the value of

pressure in the regions 3 and 4 is computed by solving numerically the following equation:

$$(p_3 - p_R)\sqrt{\frac{A_R}{p_3 + B_R}} + \frac{2c_L}{\gamma - 1}\left(\left(\frac{p_3}{p_L}\right)^{\frac{\gamma-1}{2\gamma}} - 1\right) + v_R - v_L = 0,$$

and then the pressure and the velocity are known next to the contact discontinuity. Remains to calculate the value of the density using formulas:

$$\rho_3 = \rho_L \left(\frac{p_3}{p_L}\right)^{1/\gamma}$$

and

$$\rho_4 = \rho_R \left(\frac{p_R(\gamma - 1) + p_4(\gamma + 1)}{p_4(\gamma - 1) + p_R(\gamma + 1)}\right).$$

At this time, the exact solution of (A.1) in four of five regions can be determined. For the region $i \in \{L, 3, 4, R\}$:

$$\begin{aligned}
\rho_{exact} &= \rho_i, \\
u_{exact} &= u_i, \\
p_{exact} &= p_i.
\end{aligned}$$

Finally, in the second region an exact solution is given by:

$$\begin{aligned}
\rho_{exact} &= \rho_L \left(\frac{2}{\gamma + 1} + \frac{\gamma - 1}{c_L(\gamma + 1)}\left(v_L - \frac{x - x_0}{t}\right)\right)^{\frac{2}{\gamma-1}}, \\
u_{exact} &= \frac{2}{\gamma + 1}\left(c_L + \frac{1}{2}(\gamma - 1)u_L + \frac{x - x_0}{t}\right), \\
p_{exact} &= p_L \left(\frac{2}{\gamma + 1} + \frac{\gamma - 1}{c_L(\gamma + 1)}\left(v_L - \frac{x - x_0}{t}\right)\right)^{\frac{2\gamma}{\gamma-1}}.
\end{aligned}$$

At the end, conditions which define the regions should be described. Let x_i designate the end of the i-th region, then:

$$\begin{aligned}
x_L &= x_0 + v_{head}t, \\
x_2 &= x_0 + v_{tail}t, \\
x_3 &= x_0 + v_{contact}t, \\
x_4 &= x_0 + v_{shock}t,
\end{aligned}$$

where $v_{head} = v_L - c_L$, $v_{tail} = v_3 - c_3$, $v_{contact} = v_3$ and $v_{shock} = v_R + c_R\sqrt{\frac{(\gamma+1)p_4}{2\gamma p_R} + \frac{\gamma-1}{2\gamma}}$.

APPENDIX B: Shock sensors

B.1 Shock sensor based on dilatation

The idea of the method, proposed by Bogey *et al.* in [2] for the Finite Difference (FD) scheme, is to detect regions in the domain where it is helpful to add some artificial viscosity. In this case, the viscosity is given by

$$\varepsilon = \begin{cases} \varepsilon_0 & \text{if the sensor is activated,} \\ 0 & \text{if not.} \end{cases}$$

In the following, let note $\theta = \nabla \cdot \vec{u}$ and at each node i: $\theta_i = \nabla \cdot \vec{u}_i$. First, the high-pass filtered dilatation is computed as

$$D\theta_i = -\frac{(\theta_{i+1} - 2\theta_i + \theta_{i-1})}{4},$$

and its amplitude as

$$D\theta_i^{magn} = \frac{1}{2}\left[(D\theta_i - \theta_{i+1})^2 + (D\theta_i - \theta_{i-1})^2\right].$$

Since these two definitions concern the FD approach, they have to be adapted to SD method, which is done by using the Taylor's theorem in the reference domain:

$$D\theta_i = -\frac{\nabla \cdot \nabla\theta_i}{4} \quad \text{and} \quad D\theta_i^{magn} = (\nabla D\theta_i)^2,$$

where i actually represents a flux point. Then, the sensor r is defined as

$$r_i = \frac{D\theta_i^{magn}}{c_i^2},$$

where $c_i^2 = \gamma p_i/\rho_i$ represents the square of the local sound speed. Finally, the formula of the artificial viscosity at each flux point is given by:

$$\varepsilon_i = \begin{cases} \varepsilon_0 & \text{if } \ r_i > r_{th}, \\ 0 & \text{if } \ r_i \leq r_{th}, \end{cases} \quad \text{for } \ i = 1, \ldots, d(p+2)(p+1)^{d-1}, \tag{B.1}$$

with a threshold parameter r_{th} which is used to specify the regions where the artificial viscosity should be applied.

B.2 Modified shock sensor based on pressure variations

The approach described in this section, proposed by Ducros *et al.* in [8] for the Finite Volume scheme, is similar to the previous one, only the definition of the shock sensor r changes. For now, at each node i:

$$r_i = \left| \frac{p_{i+1} - 2p_i + p_{i-1}}{p_{i+1} + 2p_i + p_{i-1}} \right| \frac{\theta_i^2}{\theta_i^2 + \|\omega\|^2 + \delta},$$

where $\delta = 10^{-30}$ is a small positive real number added to the denominator in order to prevent the division by zero and ω is the local vorticity given by

$$\omega = \begin{pmatrix} \frac{\partial w}{\partial y} - \frac{\partial v}{\partial z} \\ \frac{\partial u}{\partial z} - \frac{\partial w}{\partial x} \\ \frac{\partial v}{\partial x} - \frac{\partial u}{\partial y} \end{pmatrix}.$$

As before, the formula for Finite Volume scheme has to be adjusted to the SD approach at each flux point i by means of the Taylor's theorem:

$$r_i = \left| 1 - \frac{4p_i}{4p_i + \Delta p_i} \right| \frac{\theta_i^2}{\theta_i^2 + \|\omega\|^2 + \delta}.$$

Finally, the artificial viscosity at each flux point is defined as in Eq. (B.1).

Bibliography

[1] F. Bassi and S. Rebay. A high-order accurate discontinuous finite element method for the numerical solution of the compressible Navier-Stokes equations. *Journal of Computational Physics*, 131(2):267–279, 1997.

[2] C. Bogey, N. de Cacqueray, and C. Bailly. A shock-capturing methodology based on adaptative spatial filtering for high-order non-linear computations. *Journal of Computational Physics*, 228:1447–1465, 2009.

[3] S. Clain, S. Diot, and R. Loubère. A high-order finite volume method for systems of conservation laws - Multi-dimensional Optimal Order Detection (MOOD). *Journal of Computational Physics*, 230:4028–4050, 2011.

[4] B. Cockburn and C.W. Shu. TVB Runge-Kutta local projection Discontinuous Galerkin finite method for conservation laws II : General framework. *Mathematics of Computation*, 52(186):411–435, April 1989.

[5] S. Diot. *La méthode MOOD - Multi-dimension Optimal Order Detection - la première approche a posteriori aux méthodes Volumes Finis d'ordre très élevé*. PhD thesis, Université Toulouse 3 Paul Sabatier, 2012.

[6] S. Diot, S. Clain, and R. Loubère. Improved detection criteria for the Multi-dimensional Optimal Order Detection (MOOD) on unstructured meshes with very high-order polynomials. *Computers and Fluids*, 64:43–63, 2012.

[7] S. Diot, R. Loubère, and S. Clain. The Multidimensional Optimal Order Detection method in the three-dimensional case: very high-order finite volume method for hyperbolic systems. *International Journal for Numerical Methods in Fluids*, 73:3762–392, 2013.

[8] F. Ducros, V. Ferrand, F. Nicoud, C. Weber, D. Darracq, C. Gacherieu, and T. Poinsot. Large-Eddy Simulation of the Shock/Turbulence Interaction. *Journal of Computational Physics*, 152:517–549, 1999.

[9] A. Gelb and E. Tadmor. Detection of edges in spectral data. *Journal of Applied and Computational Harmonic Analysis*, 7:101–135, 1999.

[10] E. Godlewski and P-A. Raviart, editors. *Numerical Approximation of Hyperbolic Systems of Conservation Laws*, volume 118 of *Applied Mathematical Sciences*. 1996.

[11] H.T. Huynh. A flux reconstruction approach to high-order schemes including discontinuous-Galerkin methods. In *18th AIAA Computational Fluid Dynamics Conference, 25 - 28 June, Miami, FL, AIAA Paper 2007-4079*, 2007.

[12] A. Jameson. A proof of the stability of the spectral difference method for all orders of accuracy. *Journal of Scientific Computing*, 45:348–358, 2010.

[13] A. Klöckner, T. Warburton, and J.S. Hesthaven. Viscous shock capturing in a time-explicit discontinuous Galerkin method. *Mathematical Modelling of Natural Phenomena*, 6(3):57–83, 2011.

[14] D.A. Kopriva and J.H. Kolias. A conservative staggered-grid Chebyshev multidomain method for compressible flows. Technical report, ICASE, Report 95-18 and NASA Contractor Report 195060, 1995.

[15] D.A. Kopriva and J.H. Kolias. A conservative staggered-grid Chebyshev multidomain method for compressible flows. *Journal of Computational Physics*, 125(1):244–261, 1996.

[16] M. Lemesle. Analysis of several extensions for the spectral difference method to handle discontinuity. Master's thesis, Université de Nantes, 2014.

[17] Y. Liu, M. Vinokur, and Z.J. Wang. Spectral difference method for unstructured grids I: Basic formulation. *Journal of Computational Physics*, 216(2):780–801, 2006.

[18] Y. Liu, M. Vinokur, and Z.J. Wang. Spectral (finite) volume method for conservation laws on unstructured grids V: Extension to three-dimensional systems. *Journal of Computational Physics*, 212(2):454–472, 2006.

[19] G. Lodato. High-order schemes for high-fidelity DNS and LES of complex geometries. In *CERFACS conference on High Order Spectral Difference Method*, 2014.

[20] F.D. Lora-Clavijo, J. P. Cruz-Perez, F. S. Guzman, and J. A. Gonzalez. Exact solution of the 1d Riemann problem in Newtonian and relativistic hydrodynamics. *Mexican Journal of Physics E*, 59:28–50, 2013.

[21] R. Loubère, M. Dumbser, and S. Diot. MOOD : schémas d'ordre très élevé pour les systèmes de lois de conservation hyperboliques - Multi-dimensional Optimal Order Detection. In *CERFACS seminar*, 2014.

[22] Y. Lv and M. Ihme. Taming nonlinear instability for discontinuous Galerkin scheme with artificial viscosity. In *Center for Turbulence Research, Annual Research Briefs*, 2014.

[23] P-O. Persson. Shock capturing for high-order discontinuous Galerkin simulation of transient flow problems. In *21st AIAA Computational Fluid Dynamics Conference, June 24-27, San Diego, CA. AIAA Paper 2013-3061*, 2013.

[24] P-O. Persson and J. Peraire. Sub-cell shock capturing for discontinuous Galerkin methods. In *44th AIAA Aerospace Sciences Meeting, Reno, Nevada. AIAA Paper 2006-0112*, 2006.

[25] W.H. Reed and T.R. Hill. Triangular mesh methods for the neutron transport equation. Technical report, Los Alamos National Laboratory, New Mexico, USA, Tech. Report LU-UR-73-279, 1973.

[26] A. Sheshadri and A. Jameson. Shock detection and capturing methods for high order discontinuous-Galerkin finite element methods. In *32nd AIAA Applied Aerodynamics Conference, Atlanta, GA, June 16-20, AIAA Paper 2014-2688*, 2014.

[27] G.A. Sod. A survey of several finite difference methods for systems of nonlinear hyberpolic conservation laws. *Journal of Computational Physics*, 27:1–31, 1978.

[28] Y. Sun, Z.J. Wang, and Y. Liu. High-order multidomain spectral difference method for the Navier-Stokes equations on unstructured hexahedral grids. *Communications in Computational Physics*, 2(2):310–333, 2007.

[29] J. Trangenstein. *Numerical Solution of Hyperbolic Conservation Laws*. 2008.

[30] K. Van den Abeele, C. Lacor, and Z.J. Wang. On the stability and accuracy of the spectral difference method. *Journal of Scientific Computing*, 37:162–188, 2008.

[31] Z.J. Wang. Spectral (finite) volume method for conservation laws on unstructured grids: Basic formulation. *Journal of Computational Physics*, 178(1):210–251, 2002.

[32] Z.J. Wang, Y. Liu, G. May, and A. Jameson. Spectral difference method for unstructured grids II: Extension to the Euler equations. *Journal of Scientific Computing*, 32:45–71, 2007.

[33] M. Yu and Z.J. Wang. Shock capturing for correction procedure via reconstruction methods using artificial viscosity and diffusivity. In *The Eighth International Conference on Computational Fluid Dynamics (ICCFD8), Chengdu, Sichuan, China, July 14-18, Paper ICCFD8-2014-0079*, 2014.

[34] M. L. Yu, F. X. Giraldo, M. Peng, and Z. J. Wang. Localized artificial viscosity stabilization of discontinuous Galerkin methods for nonhydrostatic mesoscale atmospheric modeling. *Monthly Weather Review*, 143(12), 2015.